Leaf Temperatures and Physiological Vulnerability of a Tropical Forest in Western Ghats

A thesis
Submitted towards the partial fullfilment of
BS-MS dual degree programme
by

AKHIL JAVAD

Date: 18/12/2023

under the guidance of

Dr. DEEPAK BARUA
IISER Pune, India
&
Prof. EMANUEL GLOOR
University of Leeds, UK

from Jan 2023 to Oct 2023

Indian Institute of Science Education and Research
Pune

Certificate

This is to certify that this dissertation entitled "Leaf Temperatures and Physiological Vulnerability of a Tropical Forest in Western Ghats" submitted towards the partial fulfillment of the BS-MS degree at the Indian Institute of Science Education and Research, Pune represents original research carried out by Akhil Javad at Indian Institute of Science Education and Research, Pune, under the co-supervision of Dr. Deepak Barua, IISER Pune and Dr. Emanuel Gloor, University of Leeds, during academic year January 2023 to October 2023.

Supervisor:
Dr. Deepak Barua
Associate Professor
IISER Pune, India

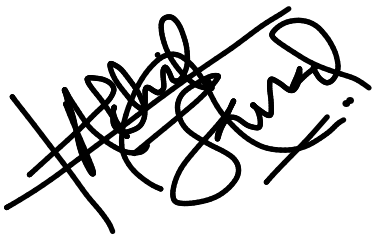

Akhil Javad
2018 1049
BS-MS
IISER Pune

Co-supervisor:
Prof. Emanuel Gloor
Professor
University of Leeds, UK

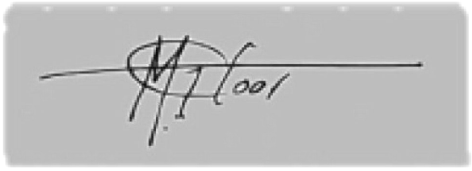

Date: 18/12/2023

This thesis is dedicated to my
Mum and Dad

Declaration

I, hereby declare that the matter embodied in the report titled "Leaf Temperatures and Physiological Vulnerability of a Tropical Forest in Western Ghats" is the results of the investigations carried out by me at the Indian Institute of Science Education and Research from the period 01-01-2023 to 20-10-2023 under the co-supervision of Dr. Deepak Barua, IISER Pune, and Dr. Emanuel Gloor, University of Leeds, and the same has not been submitted elsewhere for any other degree.

Supervisor:
Dr. Deepak Barua
Associate Professor
IISER Pune

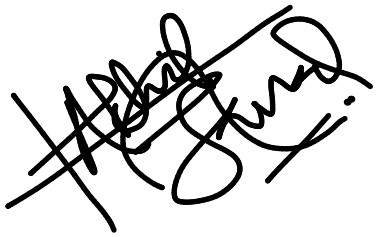

Akhil Javad
2018 1049
BS-MS
IISER Pune

Co-supervisor:
Prof. Emanuel Gloor
Professor
University of Leeds, UK

Date: 18/12/2023

Acknowledgements

I would especially like to wholeheartedly thank my supervisors, Dr. Deepak Barua and Prof. Emanuel Gloor for their guidance, encouragement and support throughout the project. I acknowledge Dr. David Galbraith for providing meaningful feedbacks and helping with the project. I thank Mr. Balachandra Hegde and Mrs. Kusuma for assistance and support during my field works. I acknowledge and thank Mr. Vikhyath Premugh and Dr. Rakesh Tiwari for their work that I have used in the study. I thank DB Lab members - Ms. Megha Ojha, Ms. Akanksha Ingale, Mr. Abhirup Khara and Mr. Omkar Kache for the hours of discussions. I recognize, and thank people who have assisted me in the field, and everyone else who had helped me along the way. I thank Department of Science & Technology, Government of India for the INSPIRE scholarship that partially supported my studies for the past 5 years. I thank Natural Environment Research Council (NERC), UK for the grant NE/R005079/1 titled "Towards an Indian observatory of tropical forest response to climate change" under the NERCDMP-700 program. I also acknowledge IISER Pune for additional funding to the project.

Contributions

Contributor name	Contributor role
Akhil Javad	Conceptualization, Data Collection, Analysis, Writing - original draft preparation
Dr. Deepak Barua	Supervision, Conceptualization Ideas, Project Administration, Funding acquisition, Writing - preparation, review and editing
Prof. Emauel Gloor	Supervision, Conceptualization Ideas, Project Administration, Funding acquisition, Writing - preparation, review and editing
Dr. David Galbraith	Project Administration, Funding acquisition, Conceptualization Ideas
Vikhyath Premugh	Data Collection
Dr. Rakesh Tiwari	Data Collection
Balachandra Hegde	Data Collection
Ron Sunny	Data Collection
Peddiraju Bandaru	Data Collection
Santiago Clerici	Technical Assistance

Abstract

Global surface temperatures are increasing, and extreme weather events like heat waves are becoming more frequent and intense, posing a threat to the functioning and dynamics of tropical forests around the world. The study reports long-term, high-resolution leaf temperatures data to discuss the exceedences and continuous exposure times above physiological thermal thresholds, and further expands to evaluate potential heat-induced damages post a hot and dry period and understand the overall vulnerability of a tropical forest in Western Ghats. The leaves are consistently approaching and exceeding CO_2 assimilation thresholds spending considerable amounts of time under non-optimal temperatures. Average continuous times of exposure above $T50$ - temperature at which Photosystem II quantum yield reduces to 50% - are not yet suggestive of prevalence of irreversible damages. Estimates of thermal safety margins for 55 species using the leaf energy budget model were able to identify species that are likely to be vulnerable under current and future climate conditions. The results suggest that there is large variation in how vulnerable physiological function is to extreme temperautres, some species may be particularly sensitive to heat induced damages in future climates with increased global temperatures.

Contents

Chapter 1

Introduction

Global land and sea surface temperatures are increasing (Rahmstorf *et al.*, 2017; Hansen *et al.*, 2010) and would likely continue warming in the future trailing the rising CO_2 levels in the atmosphere. The change in climate would increase the frequency, intensity and duration of extreme weather events like heatwaves and drought (Trenberth, 2011). In the tropics, the maximum air temperatures are expected to increase by 1^oC to 2^oC in 2100 assuming a climate conscious, sustainable society and by more than 4^oC at the extremes if a totally fossil-fuel based society prevails (O'Neill *et al.*, 2016; Grose *et al.*, 2020). Forests, agriculture and urban plantations of the tropics could be severely affected by the increase in temperatures and extreme weather events leading to reduction in Carbon sequestration, and increase in tree mortality rates (Lloyd and Farquhar, 2008; Moore *et al.*, 2021; Esperon-Rodriguez *et al.*, 2022; Feeley *et al.*, 2020). Decrease in the accumulation of Carbon in the tropical forests over time (Brienen *et al.*, 2015) given that these are one of the major Carbon sinks of the world (Pan *et al.*, 2011) further demonstrates the necessity to study the status of the tropical forests in an increasingly warming world.

Processes such as photosynthesis, respiration and stomatal closure are highly sensitive to leaf temperature (Berry and Bjorkman, 1980; Lloyd and Farquhar, 2008; Lin *et al.*, 2015). Thus, it is one of the major controls of growth and development of a plant. Peak solar radiation with insufficient cooling often leads to leaves reaching temperatures much higher than that of air (Cook *et al.*, 2021; Fauset *et al.*, 2018; Still *et al.*, 2022). Physiological thresholds such as optimum (T_{opt}) and maximum (T_{max}) leaf temperatures of CO_2 assimilation and, T_5 and T_{50} - temperatures at which quantum efficiency of Photosystem II falls to 5% and 50% respectively -

are generally used to characterize the responses of photosynthesis and carbon uptake to leaf temperature (Sastry and Barua, 2017; Slot *et al.*, 2021; Mau *et al.*, 2018). Having measures or estimates of leaf temperatures at high spatial and temporal scales across species would thus be essential in understanding vulnerability of forests to thermal stress, as well as impacts of extreme temperatures and warming at individual and community levels.

Several studies have already shown leaf temperatures either approaching or exceeding these physiological thresholds (Doughty and Goulden, 2008; Kunert *et al.*, 2022; Miller *et al.*, 2021; Araújo *et al.*, 2021; Doughty *et al.*, 2023). Studies have reported leaves experiencing temperatures 10^oC to even as high as 18^oC warmer than that of air (Fauset *et al.*, 2018; Doughty and Goulden, 2008). Although some studies are optimistic about the potential performance of tropical forests under warming via acclimation and transpirational cooling (Smith *et al.*, 2020; Drake *et al.*, 2018), the impact of extreme temperatures and exceeding physiological thresholds are not clear yet. Acclimation of leaf thermoregulatory traits (Kullberg and Feeley, 2022; Kullberg *et al.*, 2023) and increase in T_{opt} by 0.35 to $0.78^oC\ {}^oC^{-1}$ as suggested by (Choury *et al.*, 2022) do not seem to be sufficient to compensate for the potential increase in temperatures over time.

In cases when leaf temperatures are not available or measuring is not feasable, leaf energy budget modelling is a particularly useful method to get estimates of leaf temperatures across species over large spatial and temporal scales. It is a process-based approach that solves for leaf temperature by accounting for the energy fluxes such as radiation, sensible heat and latent heat across the leaf surface (Jones, 2013; Bonan, 2016; Michaletz *et al.*, 2016). Air temperature, relative humidity, solar radiation, upwelling and downwelling thermal radiation are some of the major environmental parameters that go into the model (Campbell and Norman, 1998; Bonan, 2016). Leaf size, stomatal conductance, absorptivity to solar and thermal radiation, are some of the leaf thermoregulatory traits that are responsible for species-specific leaf temperatures (Jones, 2013). Stomatal conductance could further be parametrized using models to account for stomatal responses to the environment (Guo *et al.*, 2022a; Janka *et al.*, 2016). Leaf angles or orientation with respect to the Sun is an often ignored set of parameters that influences the amount of light intercepted by the leaf (Yang *et al.*, 2023).

Thus, the overall goal of the study is to measure and understand the leaf temperatures that a tropical forest in the Western Ghats experience, and

to identify species that could potentially be vulnerable to physiological thermal stress in the future. The specific objectives of this study are to,

1. Parametrize and implement, as a computer code, the leaf energy budget model
   (a) Account for leaf orientation and stomatal responses to environmental parameters
   (b) Validate the model and do sensitivity analysis to study important regulators of leaf temperature
2. Measure leaf temperatures experienced by a tropical forest in the Western Ghats
   (a) Long-term, high resolution leaf temperatures and maximum temperatures of forestry and agroforestry species
   (b) Potential heat induced damages to Photosytem II light harvesting machinery of photosynthesis and qualitative analysis of leaf necrosis post a hot and dry period
3. Estimate thermal safety margins for 55 species in the tropical forest and assess vulnerability to thermal stress under current and future warming scenarios

Chapter 2

Leaf Energy Budget Model: Paremeterization and Sensitivity Analysis

2.1 Introduction

Leaf temperature influences several physiological processes of a plant such as photosynthesis and respiration (Berry and Bjorkman, 1980; Lloyd and Farquhar, 2008). Given how leaf temperatures can be decoupled from that of air (Cook *et al.*, 2021), it is important to have measures or estimates of leaf temperatures when studying temperature thresholds to heat as opposed to the use of air temperature as a proxy for leaf (Dong *et al.*, 2017; Tserej and Feeley, 2021). Furthermore, failing to include leaf temperatures in climate models and in studies of forest productivity can lead to erroneous conclusions (Rey-Sánchez *et al.*, 2016). Leaf energy budget model is a process-based, mechanistic approach of predicting leaf temperatures by accounting energy fluxes across a leaf surface (Jones, 2013; Bonan, 2016; Michaletz *et al.*, 2016). It is particulary useful when good measures of leaf temperatures are not available, and when predicting leaf temperatures of the past and the future.

Several studies have used the model to calculate thermal safety margins - difference between a physiological threshold and maximum leaf temperature - to study the vulnerability of plants to thermal stress (Cook *et al.*, 2021; Perez and Feeley, 2020; Kullberg and Feeley, 2022). Given that the leaf temperatures ultimately affect the growth and development

of plants, studies have tried to understand the geographic distributions, habitat preferences, and productivity of plants in relation to their thermal tolerances (Rey-Sánchez *et al.*, 2016; Feeley *et al.*, 2020; Song *et al.*, 2020; Lee *et al.*, 2015). If leaf temperatures and environmental parameters such as vapor pressure deficit and light levels are known, the model can in turn be used to predict the leaf traits particulary stomatal conductance (Vialet-Chabrand and Lawson, 2019) to study patterns of water loss and CO_2 uptake. Furthermore, the parametrizations of the energy fluxes using environmental and leaf thermoregulatory traits allow detailed sensitivity analyses to pick out important regulators of leaf temperature.

Air temperature, solar radiation and relative humidity were demonstrated to be the important environmental parameters that determine the leaf temperature (Lee *et al.*, 2015; Perez and Feeley, 2020). Some studies have also used the model to explore regulatory behaviours of water use strategies suggesting a potential trade-off between thermal regulation and water loss via transpiration (Fauset *et al.*, 2018). Leaf size or effective leaf width and stomatal conductance have been suggested to be the most important thermoregulatory traits of leaf temperature (Leigh *et al.*, 2017; Feeley *et al.*, 2020). Studies have also looked at the effects of traits like absorptivity, emissivity, and parameters of stomatal conductance models in regulating leaf temperatures (Guo *et al.*, 2022b). Although leaf orientations with respect to the Sun can significantly change the amount of intercepted light by the leaf, the angles are seldom taken into account in the implementation of leaf energy budget models (Yang *et al.*, 2023). By not taking the leaf angles into consideration, it inherently assumes that the leaves are horizontal to the ground and only a few studies explicitly mention this (Kullberg and Feeley, 2022; Fauset *et al.*, 2018).

There are several implementations of the model that have been proposed. The first, and perhaps the most used version is the Penman-Monteith Equation (Monteith, 1965) derived from the linearized form of the Clausius-Clapeyron relationship to calculate evapo-transpiration (Penman, 1948). Over the years, several revisions of the equation were put forward in order to simplify the calculations and to also account for the stomatal repsponses to environmental variables, free and forced convection, net isothermal radiation and such (Janka *et al.*, 2016; Schymanski and Or, 2017; Guo *et al.*, 2022b; Monteith and Unsworth, 2013). There are also a few alternative approaches that do not use the Penman equation of evapo-transpiration but rather use a quarternary approximation (Meyers and Paw U, 1987; Michaletz *et al.*, 2015) or a lamda W function (McColl, 2020). Linearizations were primarily done to make the model simpler, easy to implement

and to reduce computational expenses. For at least three decades, computers have been efficient enough to solve the leaf energy balance (Section 2.2) without any linearizations and as such, the approximations of evapotranspiration or net-isothermal radiation can be ignored while also accounting for stomatal responses to environmental parameters (Bonan, 2016; Guo *et al.*, 2022b; Janka *et al.*, 2016).

The main objective of this chapter is to implement a leaf energy budget model that can take into account the stomatal responses to light levels, temperature, relative humidity and vapor pressure deficit as well as the relative orientations of the Sun and the leaf. An empirical model of stomatal conductance, Stewart-Jarvis (Stewart, 1988; Jarvis, 1976), was incorporated in to the model. Solar irradiance models (Shukla *et al.*, 2015) coupled with basic vector algebra using leaf and solar angles were applied to formulate an equation to estimate the intercepted light by an inclined leaf (Section 2.4). The model was then validated against measured leaf temperatures and sensitivity analyses were done to study the importance of the parameters used in the model in regulating leaf temperatures.

2.2 Leaf Energy Balance

The temperature of a leaf is determined by the energy flux across the leaf surface and the energy stored within the leaf. Radiative flux R_n, sensible heat flux C, and the latent heat or transpirative flux λE are the energy fluxes across a leaf surface (Michaletz *et al.*, 2016; Jones, 2013). If S is the stored energy which is a function of the change in leaf temperature T_l with time t, then

$$R_n - C - \lambda E = \frac{dS}{dt} \sim \frac{dT_l}{dt} \tag{2.1}$$

forms the leaf energy balance (Michaletz *et al.*, 2016).

If the leaf is at steady state, i.e., the leaf temperature does not change with time ($\frac{dT_l}{dt} = 0$), then the net energy flux across the surface should be zero (Michaletz *et al.*, 2016; Campbell and Norman, 1998; Jones, 2013). The steady state assumption is valid as the time constants of leaf temperature responses to changing climatic variables is on the order of a few seconds to a minute (Jones, 2013; Premugh, 2020).

$$R_n - C - \lambda E = 0 \tag{2.2}$$

Since several of these terms are dependent on leaf temperatures (Eqs.

2.3, 2.4, 2.5), the equation can then solved for the leaf temperature given the other parameters of the fluxes.

Energy Fluxes

Net Radiation Flux

The radiative flux comprises the solar or shortwave radiation from the Sun R_s, the thermal or longwave radiation emitted from the ground $R_{l,up}$, the sky $R_{l,down}$ and the leaf R_{emit} itself.

$$R_n = \alpha_s R_s + \alpha_l (R_{l,up} + R_{l,down}) - 2\epsilon_l \sigma T_l^4 \tag{2.3}$$

where $2\epsilon_l \sigma T_l^4$ is the thermal radiation emitted by either surfaces of a flat leaf calculated using the Stefan-Boltzmann's Law (Jones, 2013; Campbell and Norman, 1998).

Here, α_s is the absorptivity of the leaf to the solar radiation (Campbell and Norman, 1998). Leaves have higher absorptivity towards PAR or Photosynthetically Active Radiation as opposed to NIR or Near-Infra Red light. Instead of using an overall α_s as it is here, the equation can be further parametrized using the specific absorptivities and fractions of the light spectrum. Similarly, α_l is the absorptivity of the leaf surface to thermal radiation, and ϵ_l is the emissivity of the leaf.

Sensible Heat Flux

The sensible heat flux is the advective energy transfer between the leaf and the atmosphere through a thin layer of nearly stagnant, and turbulent air surrounding the leaf surface called the boundary layer. It is driven by the leaf-to-air temperature difference, and is controlled by the heat transfer through the boundary layer defined using the boundary layer conductance g_{bh} (Jones, 2013).

$$C = \rho_a \; c_{pa} \; g_{bh} \; (T_l - T_a) \tag{2.4}$$

where ρ_a is the density of air (boundary layer), c_{pa} is the specific-heat capacity of air, and T_a is the air temperature.

Latent Heat Flux

The latent heat flux or evapo-transpirative flux is the heat loss via transpiration through the stomata and the leaf boundary layer (Jones, 2013). It is driven by the amount of water in the leaf and the amount that the

surrounding air can carry (vapor pressure deficit) and is regulated by the amount of water that can escape the leaf, defined by the stomatal conductance g_s, and the rate of vapour transfer through the boundary layer, defined by the boundary layer conductance to water vapor g_{bw}.

$$\lambda E = \frac{\rho_a c_{pa}}{\gamma} g_w (e_{sat}(T_l) - e_a) \tag{2.5}$$

where γ is the psychrometric constant which relates the water vapor pressure and the air temperature (Jones, 2013), g_w is the total water vapor conductance (Eq: 2.6) (Michaletz *et al.*, 2016; Jones, 2013), $e_{sat}(T_l)$ is the saturated vapor pressure at leaf temperature and e_a is the vapor pressure of the air surrounding the leaf. Here, the difference $e_{sat}(T_l) - e_a$ constitutes the vapor pressure deficit of the leaf. The total water vapor conductance (g_w) is a function of stomatal conductance (g_s) and leaf boundary layer conductance to water vapor (g_{bw}). g_s and g_{bw} are two conductors connected in series where the water has to escape the stomata and then the boundary layer, and thus standard equations of combining conductances can be used to estimate g_w (Eq. 2.6).

$$g_w = \frac{g_s g_{bw}}{g_s + g_{bw}} \tag{2.6}$$

Leaf Boundary Layer Conductance

Boundary layer conductance to heat

The heat transfer through the boundary layer depends on the thickness of the layer and how quickly the air molecules can diffuse from the leaf surface to the atmosphere, both of which are primarily driven by the wind speed of the free air around the leaf and the characteristic dimension or effective leaf width of the leaf (Michaletz *et al.*, 2016; Jones, 2013). Effective leaf width is the diameter of the largest incircle on the leaf lamina (Leigh *et al.*, 2017). There are several models used to predict the boundary layer conductance to heat (Eqs: 2.7, 2.8, 2.9).

$$g_{bh} = 0.007(\frac{U}{L})^{0.5} \tag{2.7}$$

Eq: 2.7 calculates g_{bh} through either surfaces (Jones, 2013) in m/s unit and is generally applicable for laminar flow of air around smooth and broad leaves. It can be multiplied by a factor of 1.5 to apply for turbulent conditions (Michaletz *et al.*, 2016). It is parametrized by wind $U(m/s)$ and characteristic width $L(m)$ of the leaf.

$$g_{bh} = 0.005(\frac{U}{L})^{0.5} \tag{2.8}$$

Eq: 2.8 is a similar one that calculates one-sided boundary layer conductance (Campbell and Norman, 1998; Bonan, 2016). A rather general equation, Eq: 2.9, explicitly uses the turbulence factors using non-dimensional numbers characterizing the nature of flow, such as Nusselt's number Nu (function of turbulence), and diffusion coefficiens of heat D_As.

$$g_{bh} = \frac{D_A Nu}{L} D_h \tag{2.9}$$

A formulation of Eq: 2.9 was used by (Guo *et al.*, 2022b) where the g_{bh} was split into forced and free convection.

Boundary layer conductance to water vapour

The water that escapes stomata is then limited by the conductivity through the boundary layer. Under turbulent conditions, it can be assumed to be the same as that of boundary layer conductance to heat (Eqs: 2.10, 2.11) (Michaletz *et al.*, 2016; Bonan, 2016).

$$g_{bw,one-sided} = g_{bh,one-sided} \tag{2.10}$$

$$g_{bw,one-sided} = \frac{g_{bh,two-sided}}{2} \tag{2.11}$$

Similar to Eq: 2.9, a general equation for g_{bw} can be written as

$$g_{bw} = \frac{D_w Sh}{L} \tag{2.12}$$

where D_w is the diffusivity of water vapor in the boundary layer, Sh is a constant called the Sherwood number (a function of turbulence).

Thermal Radiation

Thermal radiation emitted by the objects surrounding the leaf are partially absorbed by the leaf. These are primarily the downwelling radiation emitted by the sky or objects like clouds in the atmosphere, as well as upwelling radiation emitted by the Earth's surface. In addition to the absorption, the leaf itself emits thermal radiation (Eq. 2.3).

Downwelling Sky Thermal Radiation

A general approach to estimate the sky thermal radiation is to apply the Stefan-Boltzmann's Law using the emissivity and the temperature of the Sky (ϵ_{sky} and T_{sky} respectively).

$$I_{l,down} = \epsilon_{sky}\ \sigma\ T_{sky}^4 \tag{2.13}$$

Often, both ϵ_{sky} and T_g are unavailable. Either climate datasets like ERA5 (msdwlwrf variable in single levels) or approximations like Eq. 2.14 (Jones, 2013) or Eq. 2.15 (Carmona *et al.*, 2014) can be used to estimate the sky thermal radiation.

$$\begin{aligned} I_{l,down,clearsky} &\approx \sigma\ (T_{air} - 20)^4 \\ I_{l,down,cloudy} &\approx \sigma\ T_{air}^4 \end{aligned} \tag{2.14}$$

where T_{air} is the air temperature in Kelvin.

$$\begin{aligned} I_{l,down} = (&-0.34+ \\ &3.36 * 0.001 * T_{air}+ \\ &1.94 * 0.001 * Rh+ \\ &0.213 * cc) * sigma * T_{air}^4 \end{aligned} \tag{2.15}$$

where Rh is the relative humidity (%), and cc is the cloud cover, a value between 0 (clear sky) and 1 (full cloud) to represent the fraction of the sky covered with clouds.

Upwelling Ground Thermal Radiation

Ground at a given temperature emits thermal radiation upwards which is intercepted by the leaf. If T_g is the temperature of the ground in Kelvin and ϵ_g is the emissivity of the ground, then the upwelling thermal radiation can be calculated using the Stefan-Boltzmann's Law as follows (Campbell and Norman, 1998),

$$I_{l,up} = \epsilon_g\ \sigma\ T_g^4 \tag{2.16}$$

2.3 Stomatal Conductance: Stewart-Jarvis Model

Stomatal conductance is the amount of water vapor that escapes from a unit area of leaf through the stomatal openings per unit time (Michaletz *et al.*, 2016; Bonan, 2016; Jones, 2013). It is usually expressed in the units of $mmols\ H_2O\ m^{-2}s^{-1}$ or in m/s. Stomatal conductance, primarily a function of the stomatal opening parameterized by stomatal density, pore length, and guard length, is highly responsive to climatic variables like solar radiation, air temperature, vapor pressure deficit, soil water potential, atmosphere CO_2, etc. (Bonan, 2016). Depending on the purpose of modeling, having a good estimate of stomatal conductance would be important.

Several models were proposed to predict stomatal conductances based on empirical response curves, or based on optimality theory of CO_2 uptake and water loss (Damour *et al.*, 2010). Stewart-Jarvis Model is an example for a model that makes use of the stomatal response curves to climatic parameters (Jarvis, 1976; Stewart, 1988). Ball-Berry Model (Ball *et al.*, 1987) and Medlyn Stomatal conductance (Medlyn *et al.*, 2011) are examples of the latter types of models. Models like the former are generally simple and easy to implement where as the latter ones can become exceptionally complicated with several assumptions (Damour *et al.*, 2010; Bonan *et al.*, 2014) and requirements of additional models to predict assimilation rates (Farquhar *et al.*, 1980; Guo *et al.*, 2022b).

Stewart-Jarvis Model

The g_s at a given set of environmental conditions are estimated using the maximum operational stomatal conductance and the response curves of g_s to the given environmental variables. The model is relatively flexible in accomodating any number of variables as long as there is sufficient confidence in the response curves. Equations 2.17, 2.18, 2.19 and 2.20 are an example of a model that parametrizes g_s using PAR, air temperature (T_{air}) and vapor pressure deficit D (Jarvis, 1976; Stewart, 1988).

$$g_s(PAR, T_{air}, D) = g_{s,max} \cdot f(PAR) \cdot f(T_{air}) \cdot f(D) \tag{2.17}$$

Where $f(PAR)$, $f(T_{air})$ and $f(D)$ are functions of PAR, T_{air} and D that return a factor between 0 and 1. The curves shown in the Fig. 2.1, defined by the Equations 2.18, 2.19 and 2.20 are examples of an implementation of

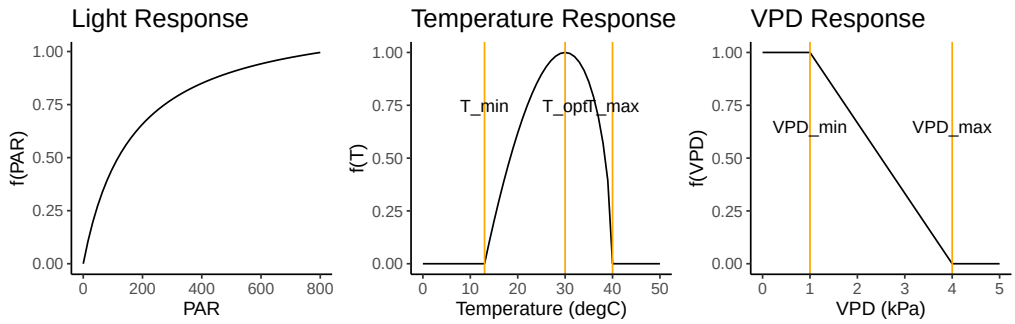

Figure 2.1: **Response curves of g_s to PAR, T_{air} and D** plotted using the equations 2.18, 2.19, and 2.20. The parameters that were used in the aforementioned equations are marked in the respective figures

the Stewart-Jarvis Model.

$$f(PAR) = \frac{d}{1 + e/PAR} \tag{2.18}$$

$$f(T_{air}) = \begin{cases} \frac{T_a - T_{min}}{T_{opt} - T_{min}} \cdot (\frac{T_{max} - T_a}{T_{max} - T_{opt}})\text{^}(\frac{T_{max} - T_{opt}}{T_{opt} - T_{min}}), & \text{if } x < 0. \\ 0, & \text{otherwise.} \end{cases} \tag{2.19}$$

$$f(D) = \begin{cases} 1, & \text{if } D < D_{min} \\ -\frac{D - D_{min}}{D_{max} - D_{min}} + 1, & \text{if } D_{min} < D < D_{max} \\ 0, & \text{if } D > D_{max} \end{cases} \tag{2.20}$$

2.4 Accounting leaf angles in absorbtion of solar radiation

Solar Radiation

Solar radiation or the shortwave is the high-energy radiation mostly in the visible, near UV and near infra-red (NIR) spectrum. For a leaf, it is the main source of energy when the other two fluxes, sensible heat flux and transpirative heat flux are in the opposite direction.

Components of solar radiation

The shortwave radiation reaching the Earth surface can be split into two components: direct, and diffuse radiation (Iqbal, 1983). Direct radiation

refers to the radiation that is coming directly from the Sun without much interference. Whereas diffuse radiation reaches the Earth through scattering in the atmosphere and reflecting off ground or, in case of a leaf, reflecting off other leaves in the canopy (Fig: 2.2). Sometimes diffuse radiation is split into diffuse radiation to account for scattered radiation coming to the Earth surface, and reflected radiation to account for the radiation reflected off of the ground (Shukla *et al.*, 2015).

On a clear day, around 10 to 30% of the global radiation at the Earth's surface constitutes diffuse radiation (Jones, 2013, pg. 22).

Leaf and Solar Angles

To calculate the light intercepted by an inclined leaf, the relative orientation of the Sun and the leaf is to be known. Angles that can define the position vectors of the leaf and the Sun in the 3 dimensional spherical coordinate system is sufficient to calculate the interception.

Leaf: The vector along the mid-rib of a leaf can be defined using two angles: zenith θ_l and azimuth ϕ_l. The former is the angle from the vertical to the mid-rib vector whereas the latter is the angle between the projection of the mid-rib vector on the ground and a vector pointing North (Fig: 2.2). For a planar leaf, these two angles are not enough as the plane can have a tilt around the mid-rib. But for most leaves of most species, this tilt is minimal and can essentially be ignored.

Sun: Sun's position vector, similar to the leaf, can be defined using the same two angles: zenith θ_s and azimuth ϕ_s (Fig: 2.2). Where θ_s is angle from the Vertical to the position vector of the Sun, and ϕ_s is the angle between the projection of the position vector on the compass plane and a vector pointing North.

It is to be noted here that the 3 dimensional coordinate system of both the leaf and the Sun should be the same with the origin at the axil of the leaf, the x-y plane parallel to the ground and the z-axis normal to the ground.

Absorbed shortwave by an inclined leaf

Several models were proposed to estimate the absorbed solar radiation by an inclined plane. Most of these models were derived primarily to calculate solar panel outputs and to get optimum angles for maximum wattage. But these models can be adapted for a leaf as the basic theories are still applicable.

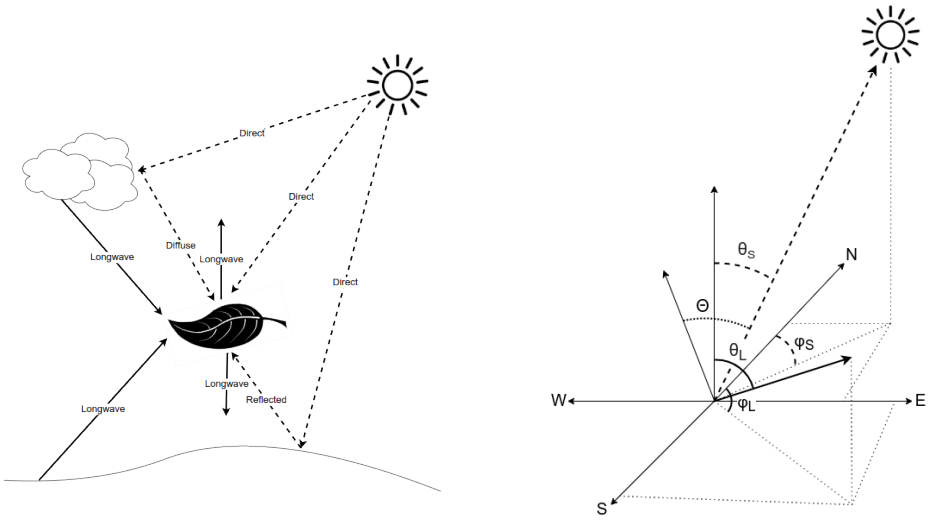

Figure 2.2: **Components of the solar radiation (left) and, Leaf and Solar Angles (right)**. Mid-rib of the leaf is the vector in bold. The dotted vector defines the position vector of the Sun. N, E, W, and S corresponds to the compass directions - North, East, West and South. θ_L and θ_S are the zenith angles of the leaf and the Sun respectively. Similary, ϕ_L and ϕ_S are the azimuth angles. Θ is the angle between the normal to the leaf's plane and the Sun's position vector..

Direct Radiation - Lambert's Cosine Law

If Θ is the angle between the surface normal and the direct light rays, then the light intercepted by the surface in question is given by the Lambert's Cosine Law (Campbell and Norman, 1998; Iqbal, 1983).

$$I_{s,dir} = I_{s,dir0} \cdot \cos(\Theta) \tag{2.21}$$

where $I_{s,dir}$ is the direct radiation intercepted by the surface and $I_{s,dir0}$ is the radiation along the direction of the sunrays.

Often, what is measured or availabe in climate data sources are the direct radiation on a horizontal surface, sometimes referred to as the Direct Normal Irradiance or DNI. For such cases, use the Sun's zenith angle to calculate the direct radiation on the incline plane.

$$I_{s,dir} = I_{s,dir,horizontal} \cdot \frac{\cos(\Theta)}{\cos(\theta_S)} \tag{2.22}$$

$\cos(\Theta)$ can be calculated assuming that the leaf lamina has no tilt around

the mid-rib, and thus, the normal to the lamina is a function of the zenith and the azimuth angles of the leaf.

$$\begin{aligned}\cos(\Theta) = &-\sin(\theta_s)\ \cos(\phi_s)\ \cos(\theta_l)\ \cos(\phi) - \\ &\sin(\theta_s)\ \sin(\phi_s)\ \cos(\theta_l)\ \sin(\phi_l) + \\ &\cos(\theta_s)\ \sin(\theta)\end{aligned} \tag{2.23}$$

Diffuse and Reflected - Liu & Jordan Model

Estimating diffuse and reflected radiation is slightly complicated and requires a few assumptions. As such, there are several models that try to predict the diffuse and reflected on an inclined surface. Isotropic models like the Liu & Jordan Model (Eqs: 2.24,2.25) (Liu and Jordan, 1960) assume a uniform distribution of diffuse radiation across the horizon whereas anisotropic models assume distributions that might have higher density of diffuse radiation along the Sun's direct rays (Iqbal, 1983).

$$I_{s,diff} = I_{s,diff,hor} \cdot \frac{1+\sin(\Theta_l)}{2} \tag{2.24}$$

$$I_{s,ref} = I_{s,global,hor} \cdot \rho_g \cdot \frac{1-\sin(\Theta_l)}{2} \tag{2.25}$$

where $I_{s,diff}$ and $I_{s,ref}$ are, respectively, the diffuse and reflected components intercepted by the leaf with zenith angle θ_l. $I_{s,diff,hor}$ is the diffuse radiation falling on a horizontal surface, also referred to as Diffuse Horizontal Irradiance or DHI, and $I_{s,global,hor}$ is the global or the overall solar irradiance on a horizontal surface.
Out of several tens of models reviewed by Shukla *et al.* (2015) and Antonanzas-Torres *et al.* (2019), Liu & Jordan Model was chosen because of its easy implementation and its relative performance.

Total intercepted solar radiation

Combining equations 2.22, 2.23, 2.24, and 2.25, the total solar radiation falling on an inclined leaf can be calculated as,

$$R_s = I_{s,dir,hor}\cdot\frac{\cos(\Theta)}{\cos(\theta_S)} + \rho_g(I_{s,dir,hor}+I_{s,diff,hor})\cdot\frac{1-cos(\theta_l)}{2} + I_{s,diff,hor}\cdot\frac{1+cos(\theta_l)}{2}) \tag{2.26}$$

Table 2.1: **Symbols and values/sources of data of the environmental parameters used in the modelling framework.** A few parameters were measured at the site (Section 2.5), and the rest comes from literature and global climate datasets (Section 2.5). SPA stands for Solar Positioning Algorithm.

Symbol	Parameter	Unit	Value / Data Source	Ref
T_a	Air Temperature	oC		
Rh	Relative Humidity	%		
I_s	Global Solar Radiation	Wm^{-2}		
U_{10}	Wind at 10m	ms^{-1}	ERA5 - u10, v10	a
tcc	Total cloud cover (0 to 1)		ERA5 - tcc	a
fsr	Forecast surface roughness	m	ERA5 - fsr	a
T_g	Ground temperature	Wm^{-2}	ERA5 - stl1	a
θ_s	Solar zenith	rad	SPA	b
ϕ_s	Solar azimuth (0 to 360)	rad	SPA	b
ϵ_g	Thermal emissivity of ground		0.97	
σ	Stefan-Boltzmann Constant	$Wm^{-2}K^{-4}$	$5.670344 \cdot 10^{-8}$	c
C_{pa}	Specific heat of air	$Jkg^{-1}K^{-1}$	1010	c

[a] Hersbach *et al.* (2018), [b] Reda and Andreas (2008), [c] Jones (2013)

2.5 Implementation of the Model

Environmental Parameters

All the environmental parameters of the model were either measured in the field, or taken from global climate datasets such as ERA5 (Hersbach *et al.*, 2018) or from literature (Table 2.1).

Field Measurements

We set up a weatherstation (HOBO H21-002 Microstation) to measure air temperature (S-TMB-M002), relative humidity and PAR (S-LIA-M003), during the measuring period. The station was setup in a mostly open area where the PAR sensors were not obstructed by any objects. Both the temperature sensor and the humidity sensor were placed inside a non-aspirated radiation shield. The data were logged from 14 Feb, 2023 to 20 June, 2023 at 10 minute frequency (Fig. 2.3).

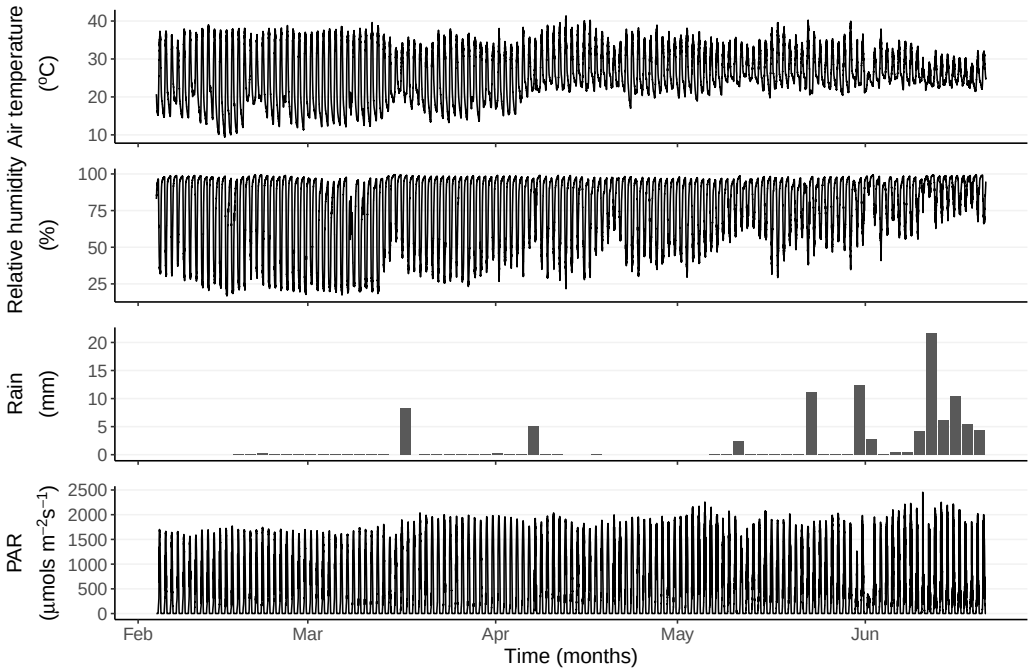

Figure 2.3: **Environmental parameters measured at the tropical forest in Sirsi, India** (Chapter 3). From top to bottom, air temperature, relative humidity, precipitation (bin width = 2 days), and photosynthetically active radiation (PAR)

Global climate data - ERA5

Climate variables, in addition to air temperature, relative humidity and PAR, that were required for leaf energy budget modelling (Table 2.1) were taken from ERA5 (Hersbach *et al.*, 2018), produced by European Centre for Medium-range Weather Forecasts (ECMWF). This global reanalysis dataset is available at a spatial resolution of 0.28^o ($\sim 31km$), and at a temporal resolution of 1 hour. Wind at $10m$ (u10, v10), total cloud cover (tcc), ground temperature (stl1) and forecast surface roughness (fsr) were downloaded for the fieldsite.

Leaf Traits

Several leaf traits are used in the model. Symbols and values or data sources of all the leaf traits are given in Table 2.2. Effective leaf width is used in the calculation of boundary layer conductance (Eq. 2.7). Absorptivities and emissivity used in the calculations of radiation (Section 2.2, 2.4) were taken from literature. Traits used in the Stewart-Jarvis Model (Section

2.3) were taken from previous studies at the site and from literature.

Table 2.2: **Symbols and values/sources of data of the leaf traits used.** Several traits were measured (Chapter 3) while the rest were taken from literature.

Symbol	Parameter	Unit	Value / Data Source	Ref
L	Effective leaf width	m		
g_s	Stomatal conductance	ms^{-1}		
ϵ_l	Thermal emissivity of leaf		0.95	a
			0.98	b
α_s	Absorptivity of leaf to shortwave		0.5	c
α_l	Absorptivity of leaf to longwave		$= \epsilon_l$	c
θ_l	Zenith angle of leaf mid-rib	rad		
ϕ_s	Azimuth angle (0 to 360)	rad		
g_{smax}	Maximal stomatal conductance	ms^{-1}		
T_{max}	Temperature threshold of g_s	^oC		
T_{opt}	Optimum temperature of g_s	^oC		

[a] Richardson *et al.* (2021), [b] Michaletz *et al.* (2016), [c] Jones (2013)

Calculated parameters

A few parameters of the model require additional assumptions or standard equations (Table 2.3). Wind at $10m$ and surface roughness from ERA5 were used to calculate the wind at $2m$ assuming a logarithmic wind profile (Tennekes, 1973; Fleagle and Businger, 1980).

$$U = U_{10} \cdot ln(2/fsr)/ln(10/fsr) \tag{2.27}$$

where U_{10} is the wind at $10m$, and $fsr(m)$ is the surface roughness (Table 2.1). 2 and 10 in the equation refers to heights $2m$ and $10m$ respectively.

A form of the Clausius-Clapeyron equation was used to calculate the saturated vapor pressure at temperature T (Eq. 2.28) (Murray, 1967; McColl, 2020). A standard equation is used to convert relative humidity into vapor pressure in air (Eq. 2.29) (Janka *et al.*, 2016).

$$e_{sat}(T) = 610.8 \ \exp(\frac{17.27\ T}{T + 237.3}) \tag{2.28}$$

where T is the temperature in ^oC.

$$e_a = e_{sat}(T_a) \cdot Rh/100 \tag{2.29}$$

Table 2.3: **Equations or models used to calculate additional parameters of the model.** Calculation of Wind at 2m assumes a logarithmic vertical profile. Equations for e_{sat}, ρ_a, and γ are standard equations/approximations used in the literature.

Symbol	Parameter	Unit	Equation	Ref
U	Wind at 2m	ms^{-1}	Eq: 2.27	a
$e_{sat}(T)$	Saturation vapor pressure at T (K)	Pa	Eq: 2.28	b
e_a	Vapor pressure of air	Pa	Eq: 2.29	c
$\rho_a(T_a, Rh)$	Density of Air	kgm^{-3}	Eq: 2.31	d
γ	Psychrometric constant	PaK^{-1}	Eq: 2.30	d
g_{bh}	Boundary layer conductance	ms^{-1}	Eq: 2.7	d,e
g_{bw}	Boundary layer conductance to water	ms^{-1}	$= g_{bh}$	e
g_w	Total water vapor conductance	ms^{-1}	Eq: 2.6	e

[a] Tennekes (1973); Fleagle and Businger (1980), [b] Murray (1967)
[c] Janka *et al.* (2016), [d] Jones (2013), [e] Michaletz *et al.* (2016)

Both psychrometric constant and the density of air were calculated (Eqs. 2.30, 2.31) based on the table given by (Jones, 2013).

$$\gamma = 64.904 \cdot 0.644(T_a - 273.15) \tag{2.30}$$

$$\begin{aligned} \rho_a(T_a, Rh) = (&1.2898 - 0.0041 \cdot (T_a - 273.15) - \\ &1.2897 - 0.0049 \cdot (T_a - 273.15)) \cdot \\ &Rh/100 \end{aligned} \tag{2.31}$$

Where ρ_a is the density of air (kgm^{-3}), T_a is the air temperature (^oC), and Rh is the relative humidity (%)

2.6 Validation of the Model

The validity of the model was tested against long-term leaf temperatures measured at a minute frequency in a tropical forest in Sirsi, India (Chap-

Table 2.4: **Correlations and RMSEs of modeled and measured leaf temperatures.** Pearson's r and p-values are given for the overall time series and during day time from the long-term, high resolution leaf temperature data (Chapter 3). Root mean squared errors are given for the overall time series, and day and night times separately. Individual names correspond to CD as *Canthium dicoccum*, MU *Memecylon umbellatum*, OD *Olea dioica*, and TP *Terminalia paniculata*. *** corresponds to $p < 0.001$

Individual	Pearson's r Overall	Pearson's r Daytime	RMSE Overall (^oC)	RMSE Daytime (^oC)	RMSE Nighttime (^oC)
CD91	r = 0.97 ***	r = 0.88 ***	1.91	2.80	0.77
CD91L2	r = 0.97 ***	r = 0.93 ***	1.72	2.43	0.90
CD250	r = 0.97 ***	r = 0.88 ***	1.69	2.30	1.03
CD1	r = 0.95 ***	r = 0.89 ***	3.16	4.72	1.08
MU34	r = 0.98 ***	r = 0.96 ***	2.32	3.26	1.28
MU34L2	r = 0.92 ***	r = 0.8 ***	2.24	3.29	0.92
MU132	r = 0.88 ***	r = 0.61 ***	3.09	4.63	1.00
OD325	r = 0.96 ***	r = 0.92 ***	1.67	2.44	0.74
OD344	r = 0.98 ***	r = 0.93 ***	1.48	2.15	0.66
OD301	r = 0.96 ***	r = 0.88 ***	1.57	2.18	0.92
OD360	r = 0.97 ***	r = 0.89 ***	1.62	2.33	0.78
TP349	r = 0.97 ***	r = 0.93 ***	2.35	3.54	0.66
TP350	r = 0.98 ***	r = 0.92 ***	1.02	1.42	0.58
TP1	r = 0.98 ***	r = 0.95 ***	1.36	1.80	0.94

ter 3). The temperatures were measured using thermistors attached on 14 leaves of 4 forestry species - *Canthium dicoccum*, *Memecylon umbellatum*, *Olea dioica* and *Terminalia paniculata*. Air temperature and light levels (PAR) were also measured (Chapter 3). Relative humidity was measured for the site whereas the rest of the environmental parameters were taken from ERA5 (Hersbach *et al.*, 2018) (Section 2.5, Table 2.1). Effective leaf width, and angles were measured while the rest were taken from literature and previous studies (Section 2.5, Table 2.2).

Across the 14 leaves, overall, the model is able to predict leaf temperatures well, although the agreement is better during night than daytime. (Table 2.4). The overall RMSEs range between 1.02^oC for TP350 to 3.16^oC for CD1 where as the daytime RMSE range from 1.42^oC to 4.72^oC. Nighttime RMSEs are the least ranging from 0.58^oC to 1.28^oC. TP1 ($r = 0.98$, $p < 0.05$), MU34 ($r = 0.96$, $p < 0.05$), CD91L2 ($r = 0.93$, $p < 0.05$), OD325

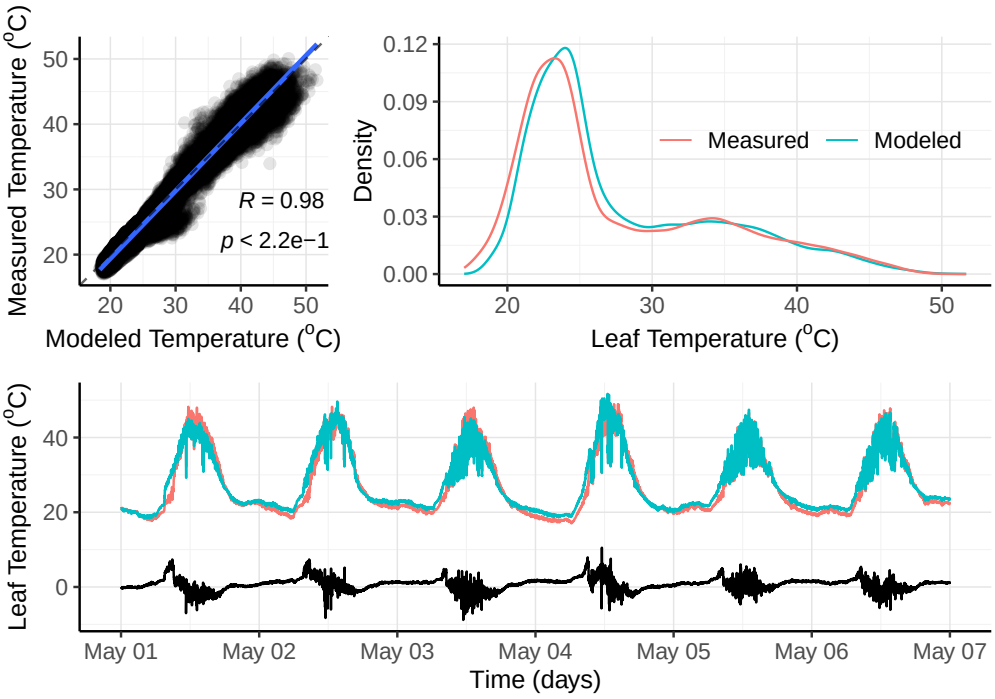

Figure 2.4: **Comparison of modeled and measured leaf temperatures of a *Terminalia paniculata* leaf**. Top left panel shows scatter of measured and modeled leaf temperatures at 1 minute frequency between April 29, 2023 and May 30, 2023 and the densities for the same are shown on the top-right panel. Bottom panel shows the traces of measured (red) and modeled (blue) for a few days incuding the difference (black) between the two.

(r = 0.92, p < 0.05) and TP350 (r = 0.92, p < 0.05) are some of the individual leaves that showed the best correlation between the modeled and the measured leaf temperatures as well as the least root mean squared errors (RMSEs) during daytimes. Predictions of CD1 (r = 0.89, p < 0.05), MU132 (r = 0.61, p < 0.05) and to some extend, TP349 (r = 0.92, p < 0.05), showed the worst agreement with the observed temperatures during the daytime having RMSEs of 4.72^oC, 4.63^oC and 3.54^C respectively.

Scatter plots, distributions and time series of modeled and measured leaf temperatures of the TP1 leaf for a few consecutive days are given in Fig. 2.4. The scatter plot, and the distributions of measured and modeled leaf temperatures showed very good correlation for this particular leaf where the model was able to pick up the lower end and the higher end of

the leaf temperatures relatively well although the variance at warmer temperatures is slightly higher compared to cooler temperatures. The differences between modeled and measured leaf temperatures showed large deviations during the daytime, particulary during peak solar hours, in contrast to the night time when the temperatures were relatively stable. A couple of hours before noon was consistently associated with overestimation of leaf temperatures across the six days (bottom panel in Fig. 2.4). During the peak time when leaf temperatures were very high and the Sun was directly up in the Sky, the differences tend to fluctuate around zero while occassionally hitting temperature differences of around 9^oC as well as -8^oC.

For four leaves (TP1, MU34L2, CD91 and OD344), modeled and measured leaf temperatures, air temperatures, and PAR used in the leaf energy budget modeling of the respective leaves are shown for a short duration of a day in Fig. 2.5. As for TP1, modeled and measured leaf temperatures showed excellent correspondence with the PAR that was used to estimate the solar radiation absorbed by the leaf (Table 2.1, Fig. 2.5). But for the other 3 leaves shown in the same figure, the PAR had dropped considerably towards the evening, around $3PM$ to $4PM$ and the same was reflected in the leaf temperature predictions during those times. Similar patterns of near zero PARs and worse agreement with measured temperatures can be seen towards the late forenoon as well, before $12PM$. Furthermore, during peak solar hours, $1PM$ to $3PM$, the model was able to do well when the measured leaf temperatures and PAR are in good agreement with each other (first panel in Fig. 2.5) whereas it overestimates when PAR recorded high light levels that was not reflected by the leaf ($3PM$ peak in the top-right panel in Fig. 2.5) and underestimates when the leaf had continued recieving sun light, meaning no reduction in leaf temperatures, but the PAR sensor recorded drop in light levels (bottom right panel in Fig. 2.5).

Although leaf temperatures were measured of 14 leaves (Chapter 3), PARs were measured only for 5 leaves. For the 5 PAR sensors, except for the one nearby TP1 leaf, the sensors were not as close to a wired leaf to perfectly capture the light environment of the leaf throughout the day. During the diurnal cycles of Sun movement through the horizon, the relative position of the PAR sensor with respect to the leaf in the microtopography of the tree canopies would significantly impact the recorded light levels. Furthermore, clouds, particulary scattered clouds, lead to frequenct fluctuations of light levels that, unless reflected in the measurements of leaf temperauture and in recorded PARs, would lead to either understimation or overestimation depending on the mismatch between the amount of light

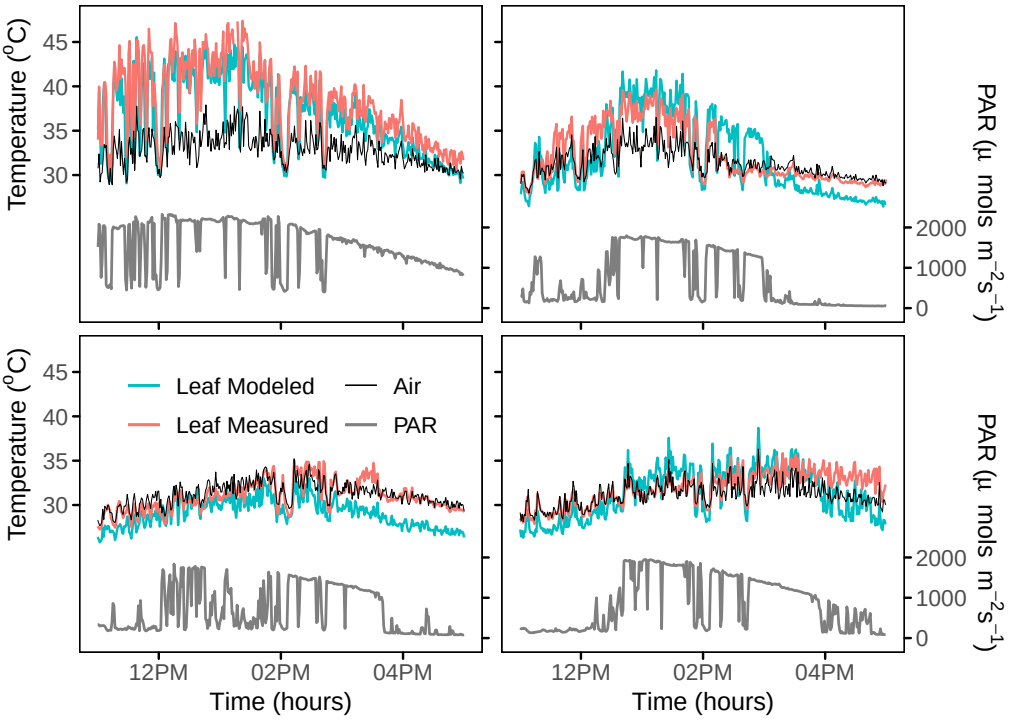

Figure 2.5: **Comparison of modeled and measured temperatures for 4 leaves during a few hours in May 03, 2023.** . Modeled (blue) and Measured (red) leaf temperatures, PAR (grey), and air temperature (black thin line) are given for leaves of - in the order of top to bottom - *Terminalia paniculata*, *Memecylon umbellatum*, *Canthium dicoccum* and *Olea dioica*.

falling on the sensor and on the leaf (Fig. 2.5). This would be worse for leaves with no PAR sensors in the vicinity. Futhermore, this could be why the TP1 with good measures of PAR had the modeled agree very well with the measured leaf temperatures. Thus, it can be speculated that fluctuations in the difference between modeled and measured leaf temperatures and the not as close agreement between the two during the day time could be due to the mismatch of light levels particulary at the temporal resolution followed in the current modeling framework.

2.7 Sensitivity Analysis

Sensitivity analyses were done to study the relative importance of parameters of the leaf energy budget model to explain the uncertainty in the pre-

dicted leaf temperatures. A sensitivity measure, β^2 Saltelli et al. (2005), was used to study the contribution of a few parameters to the variance in leaf temperatures produced by a Monte Carlo simulation (Figs. 2.6, 2.7). Particularly, the impacts of wind, cloudcover (tcc) and stomatal conductance (g_s) on leaf temperatures were studied. These 3 parameters were chosen as we had no actual measured data available and because the data from ERA5 was of marginal confidence given the grid size (0.25^o), time interval (1 hour) and the fluctuations at short temporal and spatial scales (Hersbach *et al.*, 2018). Furthermore, sensitivities to leaf size, and the two leaf angles were also studied as these 3 parameters were measured in the field for each of the 14 leaves but could have errors associated with them. Currently, the analyses reported here are exploratory and are primarily addressed towards understanding the uncertainties that some of the less reliable parameters can make on leaf temperatures. More works are required to properly quantify the contributions of each parameter in the model and to ask questions regarding major drivers of leaf temperatures.

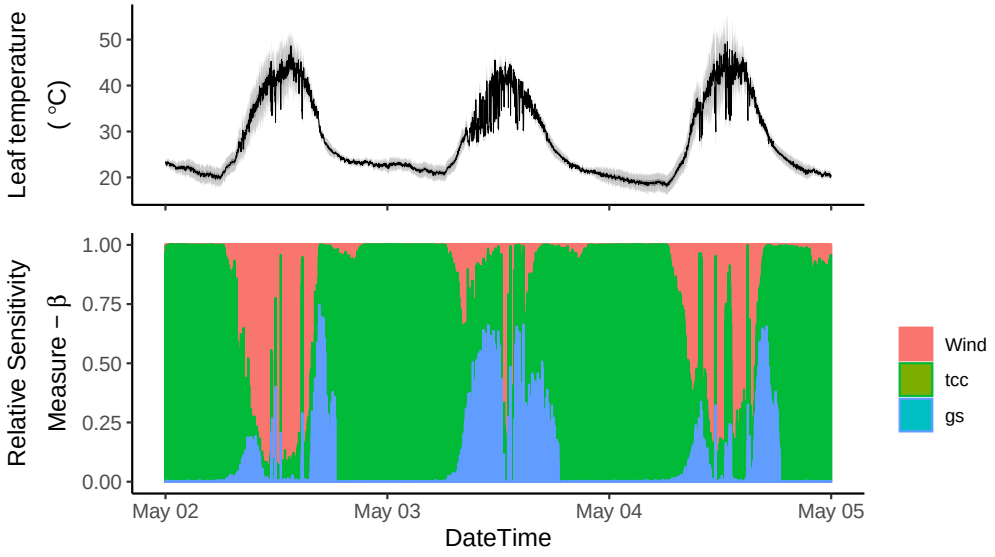

Figure 2.6: **Relative contribution of uncertainty wind, cloudcover and stomatal conductance to uncertainty in leaf temperature.** Top panel shows the leaf temperatures (black line) during the three days with the uncertainty caused by randomly sampling the three parameters from their distribution (Light grey: minimum to maximum, dark grey: mean $\pm$ SD). The relative contribution was calculated by standardizing the β^2 sensitivity measures with the sum of those of the three parameters.

At each time point (Fig. 2.6), the MC uncertainty (Monte-Carlo) was calculated by randomly sampling wind and *tcc* from their known distributions from ERA5 for that day and g_s from a distribution skewed towards zero (Section 2.3). The standard deviations and the range of the leaf temperatures produced by the MC similuations at each time step are shown as grey bands in Fig. 2.6. From this, a simple sensitivity measure, β^2, as defined by Saltelli et al. (2005) was estimated to get the relative contribution of the three parameters. β^2s were estimated as the square of the coefficients of a linear regression at a given time t (Eq. 2.32).

$$T^*_{leaf,t} = \beta_{wind,t}\ wind^*_t + \beta_{tcc,t}\ tcc^*_t + \beta_{g_s,t}\ g^*_{s,t} \tag{2.32}$$

Where $T^*_{leaf,t}$, $wind^*_t$, tcc^*_t and $g^*_{s,t}$ are the standardized ($X \rightarrow \frac{X-\mu_X}{\sigma_X}$) leaf temperature, wind, cloud cover and stomatal conductance respectively. Square of the coefficient terms $\beta^2_{wind,t}$, $\beta^2_{tcc,t}$ and $\beta^2_{g_s,t}$ then forms the sensitivity measures of wind, *tcc* and g_s respectively, at time t (Fig. 2.6).

Cloudcover contributed to the uncertainty the most at night while wind and g_s did at day times (Fig. 2.6). Cloudcover in the model impacts the thermal radiation emitted by the Sky (Carmona *et al.*, 2014) (Section 2.2). Indirectly, cloud can affect the light levels and the air temperature. Stomatal conductance influences leaf temperatures mostly during the forenoon and afternoon. At night and at times when leaf temperatures are more than 40 to 43^oC (T_{max}, Section 2.3), the stomates are closed and thus the conductance would be zero. Wind on the other hand, affects both the latent and sensible heat fluxes via boundary layer conductance to heat and watervapor (Section 2.2). At night times, the latent flux is zero and sensible heat flux is minimal.

The MC uncertainty and sensitivity measures were estimated for the measured leaf traits (Table 2.2) as well - effective leaf width, leaf azimuth and zenith angles (Fig. 2.7). Only leaf width contributed to the variation at night as leaf angles matter only when there is sunlight. During day time, both leaf width and leaf zenith impacted the leaf temperatures significantly. Leaf azimuth did not show much impact probably because the leaf was near horizontal (80^o) and such, rotation within the compass plane would not change the intercepted light as much (Section 2.4). Leaf temperatures would show large sensitivity to angles during sunrise and sunset because of the cosine rule used to calculate the intercepted light as $1/cos(\theta) \rightarrow \infty$ as $\theta \rightarrow 90^o$ (Eq. 2.26, Section 2.4). Leaf width affects the boundary layer conductance to heat and water vapour (Section 2.2). Thus at night, leaf width did not cause as much variation in leaf temperatures

as day time because the sensible and latent fluxes had been marginal. Assuming horizontal leaves could then lead to significant overestimation of leaf tempertures as reduction in light interception due to inclination with respect to the Sun rays wouldn't be captured.

2.8 Discussion

The main goal of the study was to assess whether the tropical forest tree leaves are experiencing temperatures beyond their physiological thresholds even leading to lethality. Parametrizing the leaf energy budget model for our site and species help use better understand the leaf temperatures experienced by multiple species under current and future warming scenarios and also enables to infer the key controls of leaf temperatures. The model was parametrized using climatic variables and leaf traits we mea-

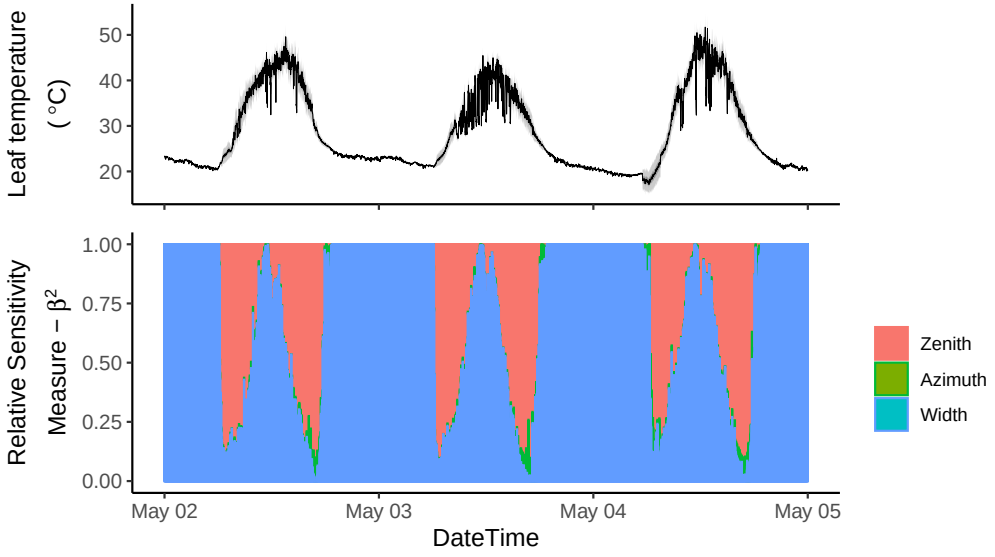

Figure 2.7: **Relative contribution of uncertainty in effective leaf width, leaf azimuth and zenith angles to uncertainty in leaf temperature.** Top panel shows the leaf temperatures (black line) during the three days with the uncertainty caused by randomly sampling the three parameters from their distribution (Light grey: minimum to maximum, dark grey: mean ± SD). The relative contribution was calculated by standardizing the β^2 sensitivity measures with the sum of those of the three parameters.

sured at the site in Sirsi, India, as well as the data from global climate datasets. The leaf temperatures measurements (chapter 3) we made were used to validate the model. Among the 3 major fluxes, solar radiation is the primary source of heat and is the significant energy term during peak solar hours as the other fluxes are often insufficient to cool the leaves. Although the net radiation term consists of thermal radiation in addition to the shortwave components (Eqs. 2.3, 2.26), the net thermal radiation is often marginal as the thermal radiation emitted by the leaf often compensates the absorbed sky and ground radiation.

Confidence in the estimated leaf temperatures depends on the accuracy of the input parameters such as air temperature, relative humidity, light levels, wind, leaf width and stomatal conductanc (Tables 2.1, 2.2) as well as the assumptions used in the parametrization of several terms in the model (Table 2.3, Eqs. 2.17, 2.15, 2.26). Parametrization of thermal radiation using the (Carmona *et al.*, 2014) and Eq. 2.16 accounted the changes in downwelling and upwelling thermal radiation as a result of changing air temperature, humidity, clouds, and ground temperature. Stewart-Jarvis model (section 2.3) (Jarvis, 1976; Stewart, 1988) was included to account for the species-specific maximal stomatal conductance (g_{smax}) and stomatal responses to leaf temperature (Eq. 2.19), vapor pressure deficit (Eq. 2.20) and PAR (Eq. 2.18). Inclusion of the effect of relative leaf orientation with respect to the Sun helped in capturing the diurnal variations in the intercepted solar radiation by the leaves as the Sun moves through the horizon with sunrays falling at varying angles on the leaf surface.

Model predictions validated against high-resolution ($1min$), long-term leaf temperature data (Chapter 3) show overall good agreement although the day time predictions, especially during peak solar hours, could have been better (Table 2.4, Fig. 2.5). The fluctuations during such times are not systematically biased towards overestimations or underestimations (Fig. 2.4). One likely reason causing the differences between modeled and measured leaf temperatures as well as deviations at certain times of day, is the mismatches between the PAR measurements and the light levels that the leaves were actually experiencing particulary at the high temporal scale ($1min$). Exploratory sensitivity analyses done to study the impact of certain parameters on leaf temperature showed wind and stomatal conductance as two parameters that could lead to large uncertainties during daytimes (Fig. 2.6), as well as leaf size and leaf angles (Fig. 2.7). Results of the current sensitivity analyses should only be taken in light of the uncertainty produced by the lack of confidence in the parameters that were studied and their distributions. These are not the appropriate metrics to

ask questions regarding the drivers of leaf temperature and the contributions of each parameter.

By parametrizing the leaf energy budget model which is based on fundamental and well understood principles and by taking into account the geometrical aspects of the absorbtion of solar radiation, the study showed that the model works very well for the site and should also work more generally. Thus, it is a reliable and a practical tool to understand the determinants of leaf temperatures and predict leaf temperatures of the future. Depending on the questions being addressed, the model can be implemented easily with simple parametrizations and it can also be made into a highly complicated model that takes into account nuanced behaviours of multiple parameters like the coupled photosynthetic and stomatal responses (Janka *et al.*, 2016; Medlyn *et al.*, 2011). Understanding and explicitly mentioning the underlying assumptions of the model could thus be important when using the model to answer different questions. More works needs to be done to study the drivers of leaf temperatures across diurnal and seasonal time scales and to study the impacts of traits such as emissivity, absorptivity, and several parameters of stomatal conductance models that are usually treated as generic constants (Guo *et al.*, 2022b; Jones, 2013). Another remaining work is to explore the parameter space to ask questions regarding "homeothermy" or regulation of leaf temperature below air temperature to primarily address why leaves do not really show homeothermy or even partial homeothermy (Chapter 3) (Still *et al.*, 2022).

Chapter 3

Measured Leaf Temperatures in a Tropical Forest of Western Ghats

3.1 Introduction

Global surface temperatures are steadily increasing due to greenhouse emissions and is expected to continue warming in the future (Rahmstorf *et al.*, 2017; Hansen *et al.*, 2010). Tropical forests would experience severe trends of rising air temperatures and extreme weather events (Doughty *et al.*, 2023; Fauset *et al.*, 2018). Although the tropical forests are one of the major Carbon sinks of the world (Pan *et al.*, 2011), forests such as the Amazon are reported to show increases in mortality rates weakening the sink (Brienen *et al.*, 2015). Several studies have already shown that tropical forests are approaching or have already exceeded photosynthetic thresholds (Doughty *et al.*, 2023; Doughty and Goulden, 2008; Mau *et al.*, 2018). The rising trend of temperature would impact the tropics at difference scales - from reduced photosynthetic activity (Moore *et al.*, 2021) to changes in species composition and distributions (Feeley *et al.*, 2020) and viable agriculturally important species. Acclimation in physiological thresholds and leaf thermoregulatory traits of the tropical species would not be sufficient to compenstate for the current rates of warming (Choury *et al.*, 2022; Kullberg and Feeley, 2022).

Leaf temperature tend to be decoupled from that of air during daytime (Campbell and Norman, 1998; Cook *et al.*, 2021) with the leaf reaching

temperatures 10 to 15^oC warmer. T_{50}s and T_5s - the temperatures at which the efficiency of Photosystem II of the photosynthetic machinery falls to 50% and 5% respectively - are the commonly used temperature thresholds of photosynthesis (Sastry and Barua, 2017; Doughty *et al.*, 2023). In order to better understand where tropical forests stand with respect to the thresholds, it is also important to have good measures of leaf temperatures at high spatial and temporal scales, and across species. Several studies have reported leaf temperature measurements at different spatial and temporal scales and using various measuring methods such as remote sensing, and thermistor/thermocouple based readings (Doughty *et al.*, 2023; Doughty and Goulden, 2008; Fauset *et al.*, 2018).

(Doughty and Goulden, 2008) showed tropical leaves reaching temperatures higher than 35^oC with leaf-to-air differences of upto 10^oC and that the CO_2 uptake, and thus, photosynthesis, being reduced at higher temperatures. Of a few studies that recorded leaf temperatures in the field conditions, (Fauset *et al.*, 2018) reported one of the highest leaf-to-air temperature differences ($\sim 18^oC$) with varying levels of thermoregulatory patterns across species although the temperatures were well below the thermal thresholds of photosynthesis. Studies such as (Araújo *et al.*, 2021) and (Doughty *et al.*, 2023) have shown that the tropical forests of the Amazonia were already were experiencing or approaching leaf temperatures above their thermal thresholds of photosynthesis and argued that it could get worse in the future and more species could experience irreversible damages to PSII.

Experiencing temperatures above thresholds like T_{50} could lead to irreversible damages to photosynthetic apparatus and could have serious consequences to growth, and development of the plants, as well as to Carbon storage and health of the forest as a whole. (Tiwari *et al.*, 2021) have argued that the photosynthetic efficiency of the Amazonia might already be affected by elevated temperatures. (Moore *et al.*, 2021) discussed the effect of increased temperatures on processes at the scales of molecules and individuals, and at ecosystem levels and raised questions about the future of crops and agriculture in a continuously warming world. (Doughty *et al.*, 2018) suggested that the leaves might darken and reduce the leaf albedo as a way to mitigate the change in climate. Acclimation in thermal thresholds as suggested by (Choury *et al.*, 2022) might not be sufficient to offset the warming the tropics currently experience and potentially in the future unless proper steps are taken. Most of the studies discussed above have leaf temperature measurements for short period of time. Having long-term leaf temperature data at high temporal resolution are necessary to understand

exposures at diurnal and seasonal scales.

Thus, the overall objective of the study was to measure the leaf temperatures experienced by a tropical forest in the Western Ghats, and put the thermal thresholds of CO_2 assimilation and PSII quantum efficiency in perspective of future climate. High-resolution, long-term leaf and air temperatures were measured for 14 leaves of 4 forestry species using thermistors. In addition, spot measurements of maximum leaf temperatures were taken for the 4 forestry species and 13 agroforestry species such as Cocoa, Cardamom, Cinnamon and Vanilla. We then analysed the exposure events above the thresholds (T_{opt}, T_{max}, T_5 and T_{50} - Table 3.3). To better understand the potential damages that the leaves might have endured during the hot and dry period of 2023, measures of PSII quantum efficiency - Fv/Fm - of sun exposed leaves and shade leaves of the forestry and agroforestry species were taken. Furthermore, a qualitative visual inspection was conducted to study any leaf necrosis on these species.

3.2 Methods

Site

Leaf temperatures were measured in a tropical forest in the Western Ghats located near Sirsi, Karnataka, India (Fig. 3.1). Situated at an elevation of $520m$, the forest experiences highly seasonal air temperature and precipitation (Fig. 3.1) where the temperatures are high during the months of March to May with little to no rain, followed by high precipitation from June to September. The leaf temperature measurements were taken during the hot and dry summer period where the temperature reaches as high as 40^oC and the precipitation near zero with occasional pre-monsoon showers towards the end of summer.

While the forests are mostly on hill tops and slopes, agricultural crops such as cocoa, vanilla, cinnamon, cardamom, clove and areca are cultivated along the valleys. We focused on 4 forestry species - *Canthium dicoccum*, *Memecylon umbellatum*, *Olea dioica* and *Terminalia paniculata* and 13 agroforestry species (Table 3.3) to measure leaf temperatures and study thermal limits and safety margins. The species were chosen based on their relative abundance in the area and their importance in the agronomy of the region. To estimate damages due to extreme temperatures, we did a set of flourometer measurements to assess the efficiency of one of the light harvesting machineries of photosynthesis (PSII), and in addition, did a coarse

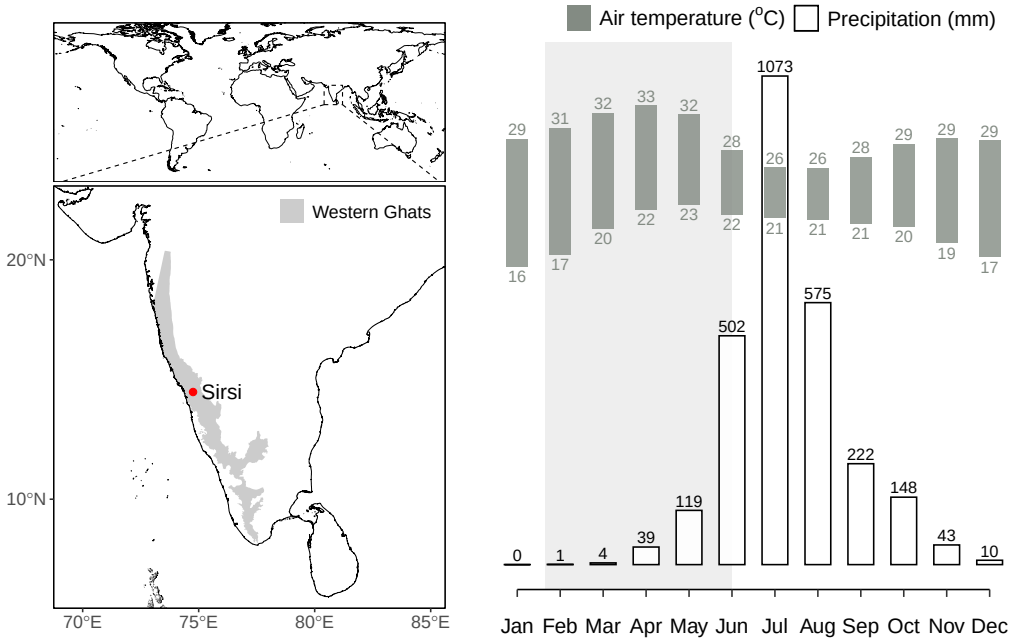

Figure 3.1: **Location of the tropical forest in the Western Ghats and climatology of minimum and maximum air temperature (grey boxes), and monthly precipitation (open bars) - CRU CL 2.0 (New *et al.*, 2002)**. Sirsi is located in the central region of the Western Ghats roughly 60km from the Arabian Sea. Measurement period is marked with a light grey box.

We measured leaf temperatures at different scales. At a canopy scale, using a thermal camera that captures images of an entire canopy of individual trees of several species (Fig. 3.2) at regular intervals. At a leaf level, we measured temperatures of 14 top-canopy, sun-exposed leaves of the 4 forestry species using thermistors attached on to the leaves. Then for the agroforestry species, a handheld thermal camera was used to get a distribution of maximum leaf temperatures during a hot week of the summer.

Thermal camera canopy temperature

A thermal camera (FLIR A2) was used to capture the thermal images of a canopy on a North-facing hillside in the field site. The images (Fig. 3.2) were taken at a frequency of 10 minutes between February 25, 2023 and June 15, 2023.

Sensitivity and Calibration of the Thermal Camera

During the month of February, 2023, several tests were done to better understand the sensitivity of the thermal camera and to account that to calibrate and thereby correct the thermal images. A black panel with high emissivity (0.95) and a panel with high reflectivity was used to do the tests by taking images of the panels through out the day while simultaneously measuring the panel temperatures using attached thermistors (Fig. 3.2). In addition to the panels, there are several leaves within the field of view that are also wired with thermistors as a part of our leaf level temeprature measurements (section 3.2). Concurrently, we also had a couple of thermistors inside the weather-proof case of the camera measuring the temperature of the camera and the air inside the case. This was done as our previous tests had shown anomalous behaviours when the temperature inside the case peaked.

Figure 3.2: **RGB and Thermal images of the canopy.** The right hand-side picture was taken on the thermal camera on 2023-03-14 12:07:22 IST. The left shows an RGB image of the same canopy. The panels, high emissivity and high reflectivity, used for calibration, can be seen at the bottom right of either images.

Long-term leaf temperature measurements using thermistors

We wired a total of 14 leaves of 3 evergreen species - (*Canthium dicoccum*, *Memecylon umbellatum*, and *Olea dioica*) and 1 deciduous species - (*Terminalia paniculata*) with thermistors (Ecomatik LAT-B2) to measure leaf temperature and air temperature at a frequency of 1 minute (Table 3.1, Fig. A.1). For 5 of the leaves, we also had sensors placed near the leaves to measure the Photosynthetically Active Radiation or PAR. The leaves

were chosen based on their position in the canopy - top canopy, sun exposed leaves, and also based on how accessbile they were.

The measurements were taken between February, 2023 and June, 2023 as this is the hottest period of the year (Fig. 3.1) except for the deciduous species (*Terminalia paniculata*) which had no leaves until the end of April and the thermistors were attached once the individuals of the species flushed the leaves. Throughout the measurement period, regular inspections were done to ensure proper functioning of the thermistors, and the data loggers. Except for a few troubles with the loggers, measurements were mostly complete throughout the period (Figs. 3.5, 3.6). In addition, we noted down the angles of all the leaves - azimuth and the zenith of the mid-rib, as well as the effective leaf width to aid in the leaf energy budget modeling (Chapter 2, Table 3.1).

Figure 3.3: **Placement of thermistors on the leaves.** Left side image shows the underside of a *Canthium dicoccum* leaf with one thermistor touching the leaf surface and the other to measure the air temperature. The right side picture shows the same leaf in its position in the canopy with the thermistors.

Intercalibration of the Thermistors

All the thermistors that were used in the study were calibrated and the data were then further corrected using a simple linear regression. The calibration was done by attaching all the thermistors on the underside of a large aluminium panel coated with black duct tape to increase the absorptivity of solar radiation. The panel was then exposed to the Sun while the thermistors measured the temperatures for a few hours. The correction was done using the mean panel temperature of all the thermistor measurements assuming a non-skewed bias around the mean.

Table 3.1: **List of leaves that were wired with thermistors.** Azimuth angle of the mid-rib of each leaf, zenith angle and the leaf width are also given. The leaves are named based on the individual tree of each species. CD: *Canthium dicoccum*, MU: *Memecylon umbellatum*, OD: *Olea dioica*, and TP: *Terminalia paniculata*. 'L2' refers to the second leaf on the same tree.

No.	Individual	Date of Placement	Azimuth (N to E) (^{o})	Zenith (^{o})	Width (cm)
1	CD250	22 Feb 2023	180.00	145.00	5.50
2	CD91	22 Feb 2023	175.00	165.00	4.50
3	CD91L2	27 Feb 2023	280.00	165.00	6.00
4	CD1	27 Feb 2023	315.00	125.00	7.50
5	MU34	5 Feb 2023	325.00	130.00	5.00
6	MU132	2 Apr 2023	300.00	120.00	4.00
7	MU34L2	2 Apr 2023	300.00	120.00	5.00
8	OD325	9 Feb 2023	280.00	135.00	4.50
9	OD360	27 Feb 2023	300.00	105.00	5.00
10	OD344	24 Apr 2023	249.00	160.00	4.00
11	OD301	25 Apr 2023	352.00	155.00	5.50
12	TP349	2 Apr 2023	245.00	120.00	5.50
13	TP350	2 Apr 2023	342.00	155.00	4.50
14	TP1	29 Apr 2023	246.00	80.00	4.50

Maximum temperatures - Forestry and Agroforestry

For 13 agroforestry species - Cardamom, Cashew, Chickoo, Cinnamon, Citrus, Clove, Cocoa, Coffee, Lemon, Pepper, Rambutan, Syzygium, and Vanilla, we measured the distribution of maximum leaf temperatures of at least 3 individuals during a few of the hottest days of the season. Measurements were done using a handheld thermal camera (FLIR C2) during $1PM$ and $3PM$ from May 08 to May 20, 2023 (Fig. 3.4).

Similary, for the 4 forestry species with the long term temperature measurements, we captured thermal images of multiple leaves, although not necessarily of the same individuals with the thermistors. Top-canopy, sun-exposed leaves were chosen in order to get a distribution of higher extreme leaf temperatures, rather than a representative for the individual as a whole. All the images were processed using *R* ((Team, 2021)) and the *Thermimage* package ((Tattersall, 2021)). The temperatures of the leaves were extracted by drawing boundaries, individually for each leaf.

Calibration of the Thermal Camera

The thermal camera (FLIR C2) was calibrated by taking images of a high-emissivity (0.95), black aluminium panel (Fig. A.2) attached with a thermistor during several times of the day. The temperature data were then corrected using a type-I linear regression (Fig. A.2).

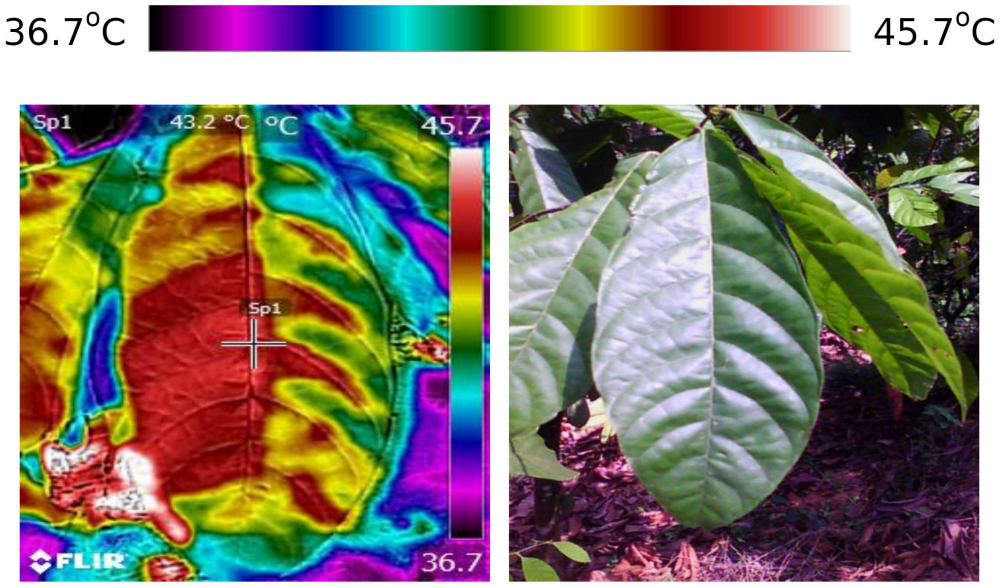

Figure 3.4: **Thermal image and corresponding RGB image of Cocoa.** Images were taken of individual leaves at a time, from a distance of 10 to 25cm. Temperatures were then extracted by drawing a mask layer around the leaf boundary using R ((Team, 2021)) and Thermimage package ((Tattersall, 2021)).

Heat damage risk assessment: Dark-adapted PSII Quantum Yield

In order to better understand the effect of high temperatures, we probed the leaves for potential heat induced damages. Two different procedures were followed. One, the photosynthetic efficiency of the leaves, the dark-adapted photosystem II quantum yield - F_v/F_m - were measured after the hot and dry period. Second, a coarse percentage of leaves with visible leaf necrosis were counted.

F_v/F_m Measurements

Photosystem II is part of the photosynthetic machinery that harvests mostly from the 680nm wavelength region of the visible light spectrum. The energy that is absorbed by PSII, particularly the pigment chlorophyll-a, drives the electron transport, with some energy lost as fluorescence and heat. A measure of the chlorophyll a fluorescence - F_v/F_m - of a dark-adapted leaf represents the maximum quantum yield of PSII (Sastry and Barua, 2017). A leaf is dark-adapted when it is kept in the dark for at least 20 minutes such that all the PSII are "open" or ready to accept photons. Here, $F_v (= F_m - F_0)$, F_m and F_0 are the variable, maximum and basal flourescence respectively. Thus, a decrease from the theoretical maximum of 0.8 represents decreased photosynthetic efficiency.

In the second to third week of June 2023, soon after the hot and the dry period, we measured F_v/F_m of sun-exposed and shade leaves of 4 forestry species - *Canthium dicoccum*, *Memecylon umbellatum*, *Olea dioica*, and *Terminalia paniculata*, and 7 agroforestry species - Cinnamon, Clove, Cocoa, Coffee, Lemon, Pepper, and Vanilla. Here, the shade leaves were taken as the controls as they experience less severe light conditions and thus cooler leaf temperatures as compared to the sun-exposed leaves. The measurements were done for 6 sun and 6 shade leaves, for 3-4 individuals of the forest species, and 5-6 individuals of the agroforestry species. All the leaves were collected early morning before 9 AM, and were then subjected to at least 2 hours of rehydration. Then they were dark adapted for at least 20 minutes followed by the measurement of F_v/F_m using PAM 2500 flourometer (Walz, Effeltrich, Germany).

Visible leaf damage

In addition to the F_v/F_m measurements, we coarsely estimated the percentage of any visible, potentially heat-induced, leaf damage or necrosis. Sun exposed leaves of at least 3 individuals were randomly counted by noting down the number of leaves with visible damage. This was done for the 4 forestry species and for 13 agroforestry species - Areca, Cardamom, Cashew, Chickoo, Citrus, Clove, Cocoa, Coffee, Lemon, Pepper, Rambutan, Syzygium, Turmeric, and Vanilla.

Physiological thresholds

Four physiological thresholds were used in the study - T_{50}, T_5, T_{opt} and T_{max} to understand the exposures of leaves above these temperatures. T_{50}

is the temperature at which the maximum quantum yield of PSII (F_v/F_m) falls by 50% and designates irreversible damages to the photosynthetic machineries (Sastry and Barua, 2017). T_5, similarly, is the temperature when it falls to 5% of the maximum chlorophyll a flourescence. Both T_{50} and T_5 values for 40 forestry and 15 agroforestry species in our field site were taken from a previous study (Premugh, 2020). Either parameteres were estimated by fitting a 4-parameter logistic regression on the F_v/F_m responses to leaf temperature at 30 minutes exposure.

T_{max} and T_{opt} are the maximum and the optimum temperature from CO_2 assimilation vs leaf temperature curves. The data for the 4 focal forestry species were taken from another study (Tiwari unpublished) in which the measurements were done using Li-Cor 6400xt on live leaves.

3.3 Results

3.3.1 High-resolution, long-term leaf temperature data

Leaf temperatures measured at high temporal resolution ($1min$) show large variations at daily, weekly and monthly scales (Figs. 3.5, 3.6). Daily maximum, and minimum leaf temperatures varied throughout the measurement period. A relatively quick increase of 5 to 6^oC in the minimum temperature was observed in the first week of April which then stayed throughout the Summer across all leaves with measurements. During March, most of the *Canthium* leaves showed a diurnal range of 25^oC which then reduced to 10 to 15^oC towards the end of the summer. Similar patterns can be seen in *Olea* as well but not with leaves of the other two species.

At diurnal scale, leaf temperatures stay close to air temperature, within 1 to 2^oC, during the nighttime, early morning and late evening (Fig. 3.7). But during the day time, especially when the Sun is directly up in the Sky, leaf temperatures are as high as 12^oC above air temperatures (Fig. 3.7). *Memecylon* leaves hit temperatures above 42^oC with leaf-to-air temperature differences being greater than 5^oC on most days, during times of peak leaf temperatures (Fig. 3.5). Leaves of the other three species, although not as high has *Memecylon*, had daily maximum temperatures above 37^oC on most days with leaf-to-air temperature differences above 2^oC.

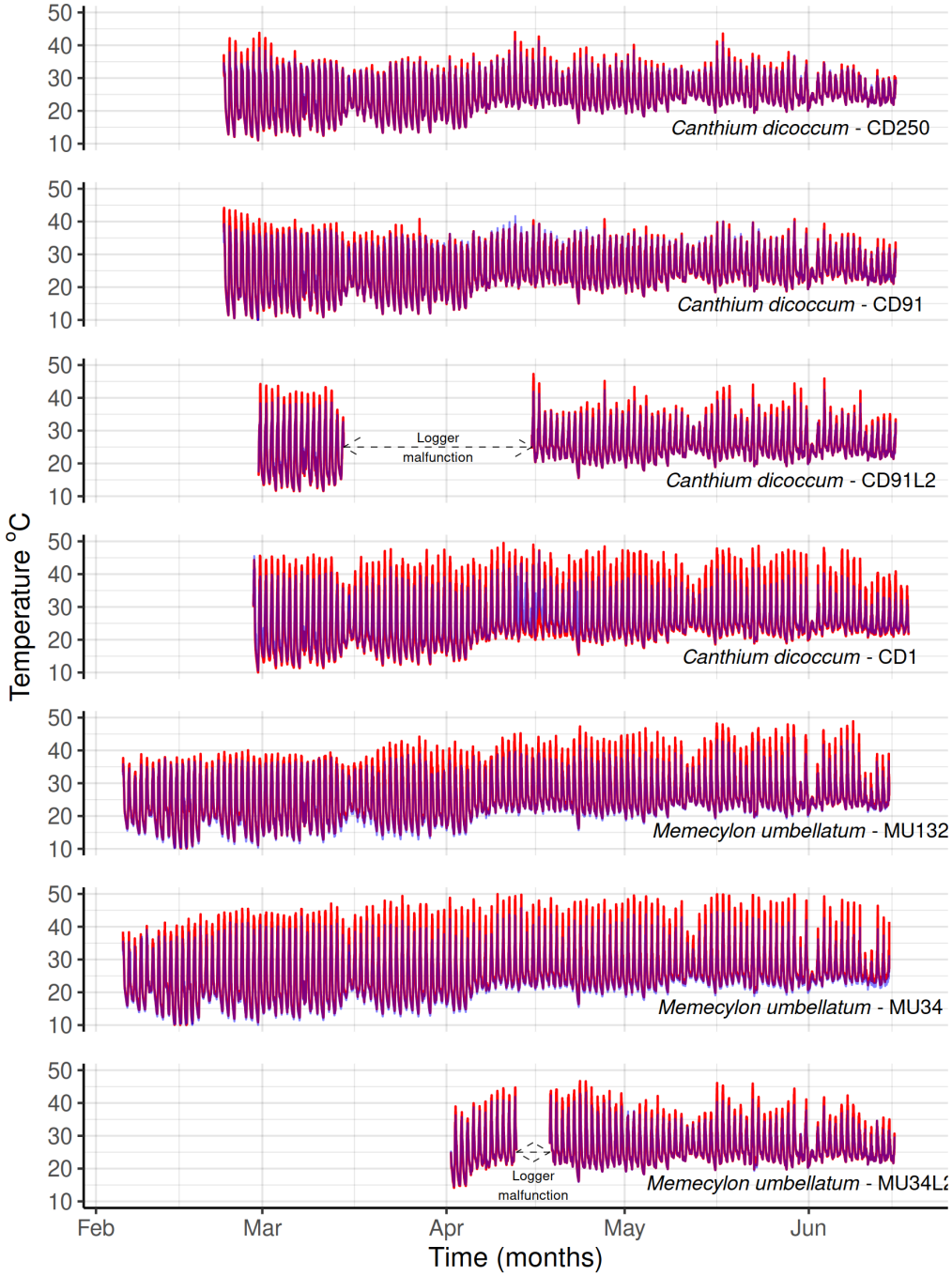

Figure 3.5: **Leaf and air temperatures measured through the Summer for *Canthium dicoccum and Memecylon umbellatum* leaves.** Leaf temperature is drawn in red and air in blue. Temperatures were measured at a minute frequency.

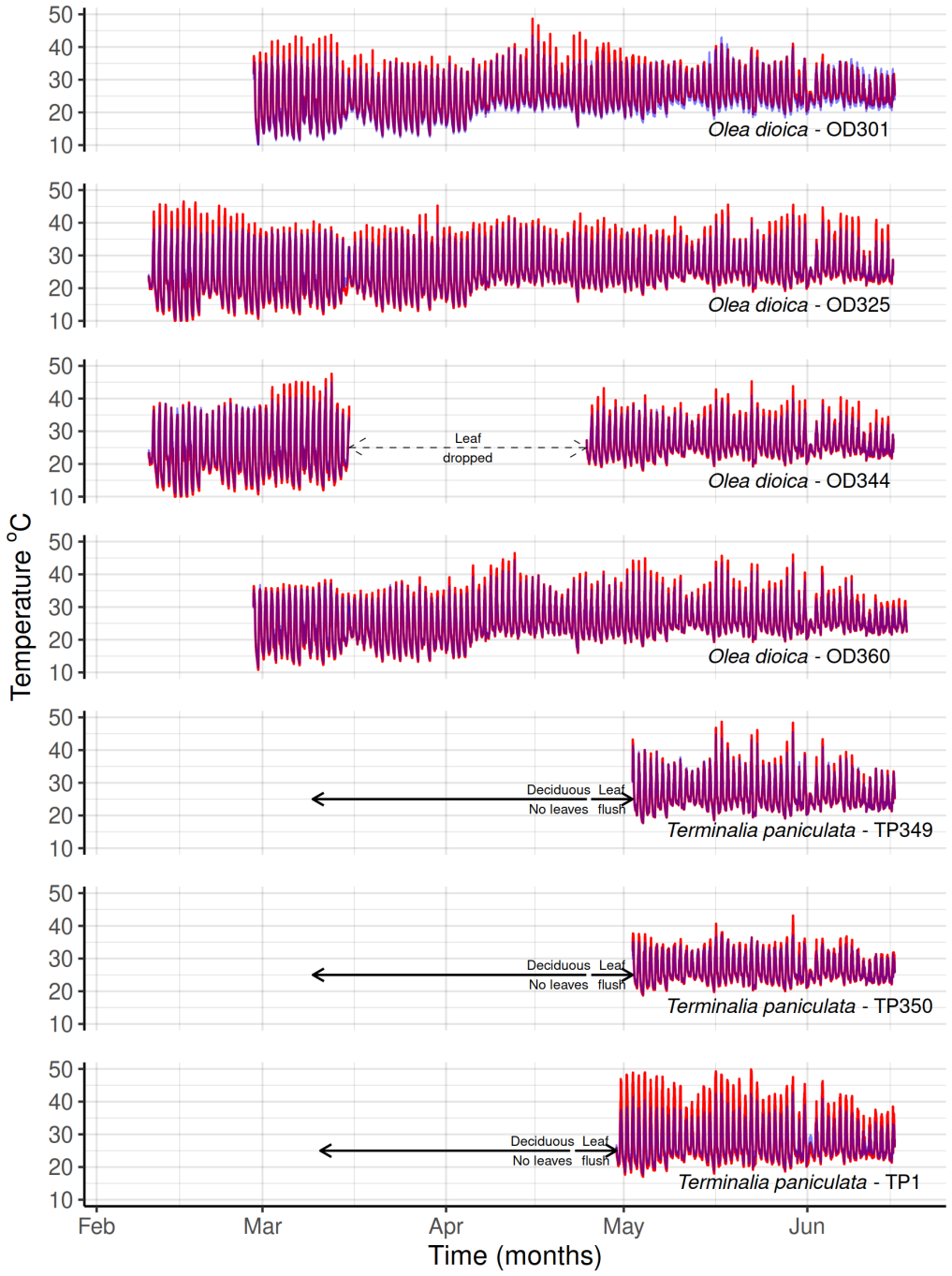

Figure 3.6: **Leaf and air temperatures measured through the Summer for *Olea dioica* and *Terminalia paniculata* leaves**. Leaf temperature is drawn in red and air in blue. Temperatures were measured at a minute frequency.

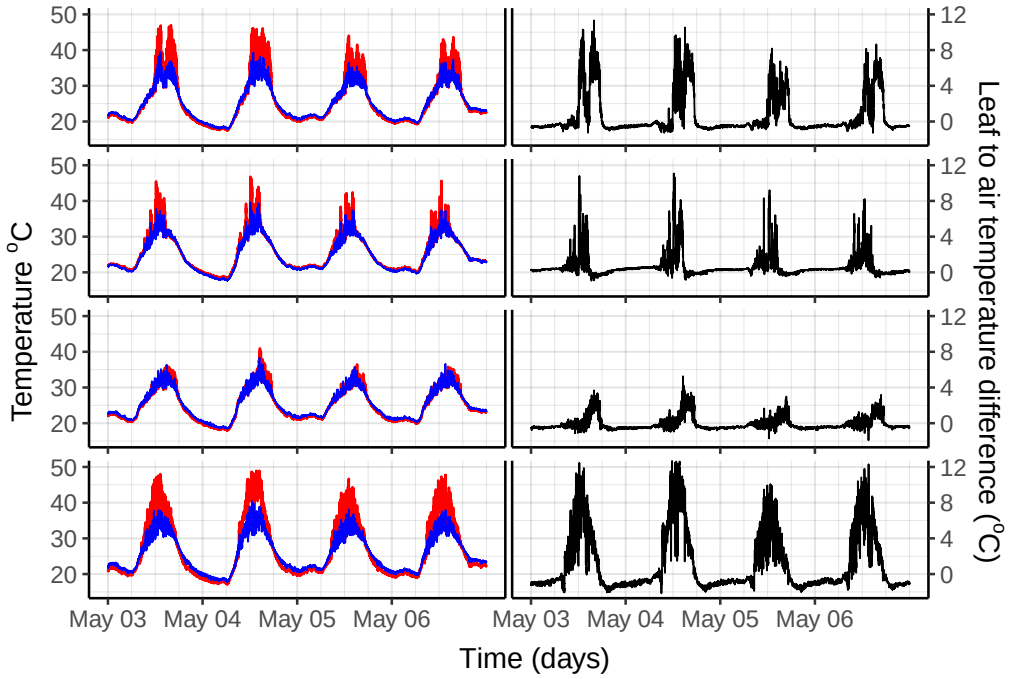

Figure 3.7: **Leaf and air temperatures (left) and corresponding leaf-to-air temperature difference (right)** of, from top to bottom, CD1, MU132, OD344 and TP1 as shown in Figs. 3.5,3.6. Leaf temperatures are in red and air temperatures are in blue.

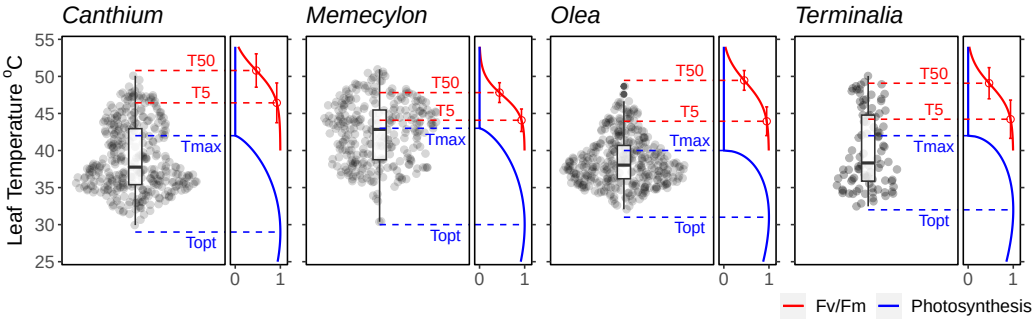

Figure 3.8: **Distribution of daily maximum leaf temperatures** from the long term time series (Figs. 3.5, 3.5) pooled from multiples leaves of each species. CO_2 assimilation curves and thresholds - T_{opt} and T_{max}, and Fv/Fm PSII response curves and thresholds - T_5 and T_{50}, are marked with blue and red lines respectively. Bars show inter-quartile range and median.

3.3.2 Maximum leaf temperatures and physiolotical thresholds

Among the four forestry species (Figs. 3.5, 3.6), *Memecylon umbellatum* and *Terminalia paniculata* occasionally exceed T_{50}s, the temperature at which the PSII efficiency reduces to half (Fig. 3.8) whereas all four species do exceed their T_5s. 14 leaves of the 4 species have their daily maximum temperatures well above their optimum temperatures for CO_2 assimilation throughout the measuring period (Fig. 3.8). For *Memecylon*, almost half of the days had peak temperatures above T_{max}, meaning no photosynthesis at those times.

Table 3.2: **Physiological thresholds of the 4 focal forestry species and the time of exposure.** Exposure is the average time in *minutes* spent by the leaf continuously above the thresholds where as the maximum exposure is the maximum time spent.

Leaf	$T_{opt}/T_{max}/T_5/T_{50}$ (^oC)	Exposure (min)	Maximum Exposure (min)	Visible Necrosis (%)
CD250	29/42/46.43/50.79	370/ 0.42/ 0 /0	496/14 /0 /0	0
CD91	29/42/46.43/50.79	410/ 0.40/ 0 /0	507/6 /0 /0	0
CD91L2	29/42/46.43/50.79	342/ 2.92/ 0 /0	439/43 /3 /0	0
CD1	29/42/46.43/50.79	355/27.62/ 1.16/0	440/62 /6 /0	0
MU132	30/43/44.08/47.81	378/ 6.48/ 3.27/0.04	500/30 /11 /1	0.22
MU34	30/43/44.08/47.81	357/46.16/29.99/3.03	475/180/130/30	0.28
MU34L2	30/43/44.08/47.81	302/ 3.10/ 0.93/0	466/8 /5 /0	0.28
OD301	31/40/43.94/49.46	242/ 2.92/ 0.31/0	431/31 /6 /0	
OD325	31/40/43.94/49.46	279/11.64/ 0.82/0	382/77 /4 /0	0.08
OD344	31/40/43.94/49.46	254/ 7.63/ 0.61/0	414/19 /5 /0	0.05
OD360	31/40/43.94/49.46	206/ 6.16/ 0.32/0	382/20 /3 /0	0.15
TP349	32/42/44.22/49.07	174/ 8.16/ 3.14/0	376/50 /24 /0	0
TP350	32/42/44.22/49.07	140/ 0.25/ 0.00/0	348/8 /0 /0	0
TP1	32/42/44.22/49.07	330/46.32/20.57/0.11	479/145/51 /1	0

The time spent consecutively above each physiological threshold were calculated for each of the 14 time series (Table 3.2). One of the *Memecylon* leaves that had several events of exceeding T_{50}s spent, on average, 3 minutes above the threshold with a maximum continuous exposure of 30 minutes. The rest of the 13 leaves barely spent any time above T_{50}s. Above T_5, only two leaves (*Memecylon* and *Terminalia*) spent any considerable

amount of time - 30 and 20 minutes respectively on average with a maximum of 130 and 51 minutes. The same two leaves, on average, spent three quarters of an hour to upto 3 hours without any CO_2 assimilation. Furthermore, all the leaves were photosynthesizing above optimum temperatures for 4 to 6 hours continuously.

The spot measurements of maximum leaf temperatures during the hot and dry period of the season were taken for 13 agroforestry species - Cardamom, Cashew, Chickoo, Cinnamon, Citrus, Clove, Cocoa, Coffee, Lemon, Pepper, Rambutan, Syzygium, and Vanilla and the 4 focal forestry species also show leaf temperatures exceeding photosynthetic thresholds - T_{50} and T_5 (Fig. 3.9). Although the data was very sparse temporally, it had more number of leaves per individual plant and species than with the long term data. Out of the 17 species probed, 6 species had at least one leaf exceeding T_{50}s and 13 species exceeding T_5s. Thresholds and percentage of exposures are given in the Table 3.3. The thermal safety margin, difference between 95th percentile leaf temperature and T_{50}, would put *Memecylon*, Cocoa and Lemon at at great risk and Syzygium and Cashew as safe. The percentage of leaves that exceeds T_{50} is relatively much higher for the three species - 29%, 23% and 13% respectively. In addition to the three species, Vanilla, Rambutan, and Chickoo show large exposure to T_5s.

3.3.3 Potential heat induced damages to leaves

PSII response as Fv/Fm is a measure of photosynthetic efficiency and a decrease from its maximum level is an indicator of heat induced damages to leaf machineries. It was measured for sun and shade leaves of 7 agroforestry species and the 4 focal forestry species soon after the hot and dry period ended (Fig. 3.10). Sun leaves show a reduction in the Fv/Fm values with respect to the Shade leaves of all species but only significant for 4 species (Table 3.4, Fig. 3.10). For Cocoa, Cinnamon and Vanilla, Sun and shade Fv/Fm values show large variation (0.5 to 0.8) and suggests hazardous levels of reduction in photosynthesis, except for the shade leaves of Vanilla.

Species level Fv/Fm values (Fig. 3.10) were compared (Fig. 3.11) with leaf temperatures (Fig. 3.9), thermal safety margins, T_{50}s, and exposures above T_{50} and T_5 (Table 3.3). Leaf temperatures and T_{50}s show mildly significant negative (r = -0.54, p = 0.085) and positive (r = 0.54, p = 0.085) correlations with Fv/Fm respectively. TSMs or thermal safety margins show a significant positive relationship with Fv/Fm (r = 0.63, p = 0.036) while exposures above T_{50} and T_5 show strong negative correlations (r =

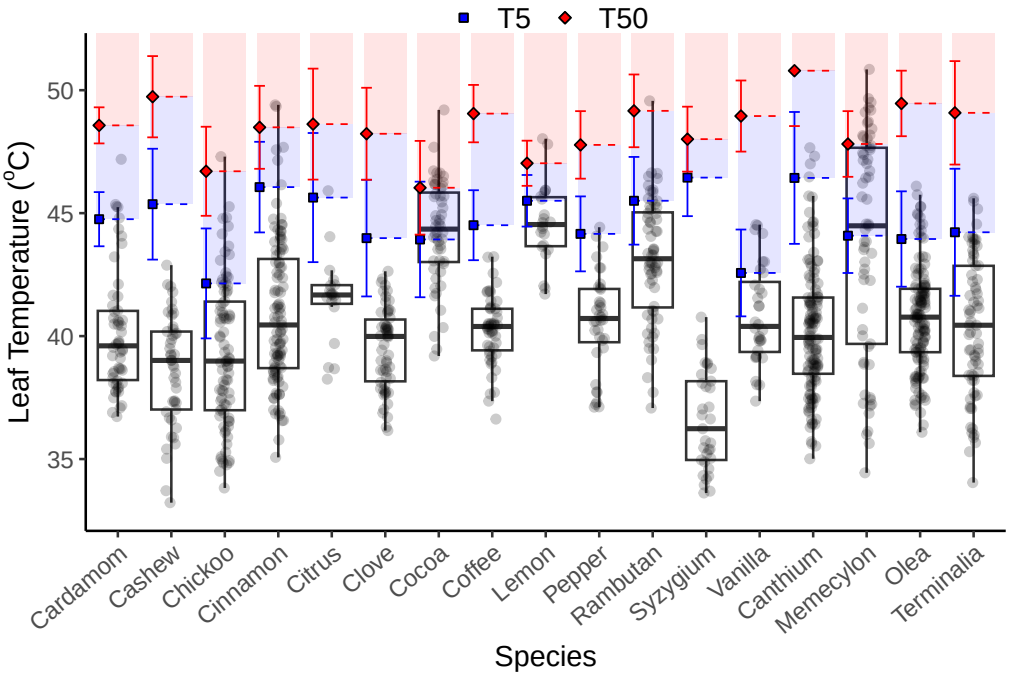

Figure 3.9: **Distribution of maximum leaf temperatures of 13 agroforestry and 4 forestry species.** Measurements were taken using a thermal camera on several sun-exposed leaves of atleast 3 individuals during the hot and dry period. Red and blue region denotes exposure to T_{50} and T_5 respectively.

-0.82, p = 0.0019 & r = -0.62, p = 0.04 repectively).

Visual inspection of leaf necrosis at the end of the summer also indicate potentially heat induced damages although the results are not conclusive of extreme leaf temperatures leading to necrotic damages. Among the agroforestry species, Rambutan showed the highest number of leaves with necrosis (42% of sun-exposed leaves) followed by Coffee (21%), Clove (15%), Cardamom (15%), Pepper (15%) and Cocoa (13%). The forestry species didn't show much necrotic damages except for *Memecylon* (21%) and *Olea* (10%). The percentage score of leaf damages here cannot be attributed solely to high leaf temperatures even though the sampling was focused to pick up heat-induced damages. The results here, thus, can only suggest indications of potentially heat related necrosis.

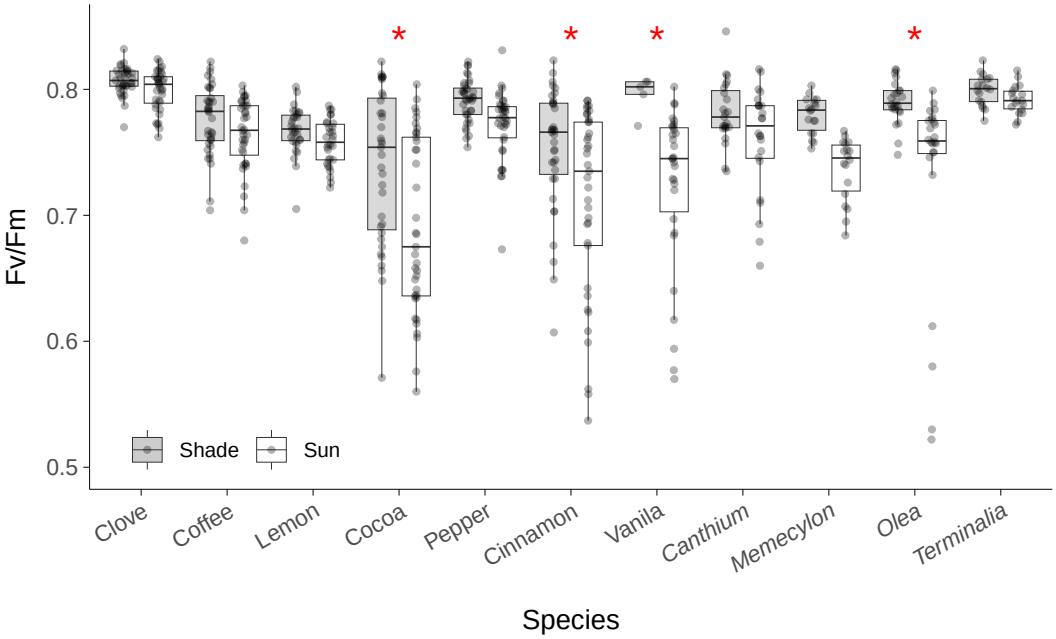

Figure 3.10: Fv/Fm **measured for sun and shade leaves of agroforestry and forestry species.** Measurements were taken during the second to third week of June after the hot and dry summer. Red stars denote species with significantly different sun and shade Fv/Fm.

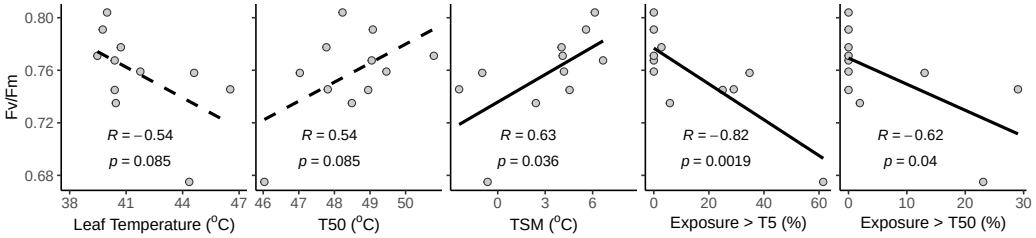

Figure 3.11: **Correlation matrix comparing Fv/Fm values and leaf temperatures, T_{50}s, and exposures** (Table 3.3). Each point is a species as shown in Fig. 3.10. TSM refers to thermal safety margin - difference between T_{50} and 95^{th} percentile leaf temperature. Exposure represents the percentage of leaves with temperatures above T_{50} or T_5. Pearson's r correlation and p value are given inside each subplot as R and p respectively.

Table 3.3: **Photosynthetic thresholds and exposures.** Leaf temperatures were taken for sun-exposed leaves of 13 agroforestry and 4 forestry species using a thermal camera. The exposure is the percentage of leaves that recorded temperatures above the respective threshold. TSM or thermal safety margin is the difference between 95th percentile leaf temperature and T_{50}.

Species	Median T_{leaf} (^oC)	T_5 (^oC)	T_{50} (^oC)	Exposure T_{leaf}>T_5 %	Exposure T_{leaf}>T_{50} %	TSM (^oC)
Cardamom	39.60	44.75	48.57	9.26	0.00	3.32
Cashew	39.01	45.36	49.73	0.00	0.00	7.76
Chickoo	38.98	42.14	46.70	18.60	1.16	2.31
Cinnamon	40.45	46.06	48.49	5.83	1.94	2.41
Citrus	41.67	45.63	48.62	5.26	0.00	4.39
Clove	39.99	43.98	48.23	0.00	0.00	6.14
Cocoa	44.35	43.93	46.03	61.54	23.08	-0.64
Coffee	40.39	44.51	49.05	0.00	0.00	6.66
Lemon	44.61	45.50	47.03	34.78	13.04	-0.98
Pepper	40.72	44.16	47.77	2.78	0.00	4.04
Rambutan	43.15	45.50	49.16	17.19	1.56	2.68
Syzygium	36.23	46.44	48.01	0.00	0.00	8.27
Vanilla	40.39	42.57	48.95	25.00	0.00	4.54
Canthium	39.47	46.43	50.79	0.00	0.00	4.11
Memecylon	46.53	44.08	47.81	29.03	29.03	-2.44
Oleo	41.75	43.95	49.46	0.00	0.00	4.19
Terminalia	39.76	44.22	49.08	0.00	0.00	5.58

Table 3.4: **Two-way ANOVA results on Fv/Fm measurements** (Fig. 3.10). SunShade represents the position of the leaf within the canopy - Sun exposed or shade. The ANOVA was nested with Individual.

```
Df Sum Sq Mean Sq F value   Pr(>F)
Species                      10 0.4504 0.04504  27.216  < 2e-16 ***
SunShade                      1 0.1142 0.11416  68.980 7.09e-16 ***
Species:SunShade             10 0.0534 0.00534   3.229  0.00046 ***
Species:SunShade:Individual  21 0.1106 0.00526   3.181 2.85e-06 ***
Residuals                   578 0.9566 0.00166
---
Signif. codes:  0 ‘***’ 0.001 ‘**’ 0.01 ‘*’ 0.05 ‘.’ 0.1 ‘ ’ 1
```

3.4 Discussion

The high-resolution, long-term leaf temperature data reported here is one of the only datasets reported so far that captured continuous thermistor measurements of leaf temperatures at high temporal resolution, across multiple leaves and through a whole summer season. The longest continuous data we have spanned a little over four months. Most studies that reported thermistor or thermocouple measurements were at short time spans of around 10 days (Rey-Sánchez *et al.*, 2016; Doughty *et al.*, 2023; Fauset *et al.*, 2018) and a lack of long term data could be attributed to the difficulties associated with measurements in the field (Aubrecht *et al.*, 2016). The data showed strong diurnal patterns where leaf temperatures were very high during day times, particulary the peak solar hours (Fig. 3.7), and also showed high seasonal patterns in maximum and minimum leaf temperatures, and diurnal ranges. The maximum leaf to air temperature differences across leaves ranged from 4^oC to 12^oC and suggests a lack of leaf homeothermy supporting recent evidences (Still *et al.*, 2022; Rey-Sánchez *et al.*, 2016; Fauset *et al.*, 2018) as evapo-transpiration and sensible heat loss were unable to compensate for the amount of solar radiation absorbed by the leaves which had been considered as the contributors of leaf thermoregulation below that of air (Michaletz *et al.*, 2015, 2016; Kullberg and Feeley, 2022).

The long term data also showed leaves consistently exceeding thermal thresholds of CO_2 assimilation (T_{max}) and occassionally approaching and exceeding thresholds of PSII quantum yield (T_{50}) - the temperature above which irreversible damages to photosynthetic machineries could prevail. The leaves spent a considerable amount of time, $2hours$ to well over $6hours$ a day on average, experiencing leaf temperatures above the optimum for CO_2 assimilation while they spent about a minute to an hour, during day time on average, potentially without any photosynthesis (Table 3.2). The maximum leaf temperatures measured for the agroforestry and forestry species further corroborate the evidences of leaf temperatures exceeding T_5s and T_{50}s the impacts of which needs to be studied in more detail. In a worst case scenario, this could mean that species like *Cocoa* and *Cinnamon* might not be able to grow in these regions and would lead to serious implications on the overall status of agriculture in the region. Although T_5 or similarly T_{crit} - temperature at which the PSII quantum yield starts to drop - is sometimes used as a hard limit on the sturdiness of photosynthetic machineries and even to leaf lethality (Doughty *et al.*, 2023), we acknowledge that T_{50}s might be a better metric as a threshold

for irreversible damages on PSII rather than T_{crit} (Sastry and Barua, 2017; O'sullivan *et al.*, 2017).

Furthermore, given the 30 minute exposure times for thermotolerance assays (Section 3.2) used in estimating T_5s and T_{50}s, the exposure times of leaves above the thresholds cannot be neglected while making conclusions of potential heat induced damages from exceedance of physiological thresholds. Currently, there was only one event that had 30 minutes of continuous exposure above T_{50} (MU34 - Table 3.2) and the average time the MU34 leaf spent continuously in a day was 3 minutes whereas the rest of the leaves barely spent time above T_{50}s. Under future warming, as leaf temperatures increase in relation to the rise in air temperatures, the events of exceedence of temperatures as well as the average and the maximum continuous exposures above the physiological thresholds could increase, and it could be worse particularly for the species such as *Cocoa*, *Cinnamon*, *Coffee*, *Rambutan*, *Lemon*, *Vanilla*, *Memecylon umbellatum* and *Terminalia paniculata* that are already exceeding or are approaching the thresholds.

The Fv/Fm measurements and qualitative visual inspection of leaf necrosis are suggestive of potentially heat-induced damages (Figs. 3.10, 3.11). After the hot and dry period of the Summer, the shade leaves, which would have experienced relatively cooler leaf temperatures in contrast to the Sun exposed ones, showed consistently higher PSII quantum efficiencies (Table 3.4). Leaves of *Cocoa*, *Cinnamon* and *Vanilla* showed large variation in the Fv/Fm values suggesting reductions in the overall photosynthetic activity. Species that recorded higher leaf temperatures and lower T_{50}s, or rather the species with low thermal safety margins showed significant decline in PSII efficieny. Additionally, the species with the highest percentage of leaves exceeding either PSII thresholds were associated with low PSII quantum yield. The visual inspection of leaf necrosis were also suggestive of heat induced damages to leaf machineries although are not sufficient to conclude that the heat is causing necrotic damages. Overall, the results strongly indicate the presence of heat-induced damages and photosynthetic declines.

The tropical forest in the Western Ghats could potentially be at risk of thermal stress as the climate steadily warms and extreme weather events like heatwaves increase in frequency and intensity. This study adds on to several recent studies from the tropical forests around the world reporting that the leaf temperatures are approaching and exceeding physiological thresholds (Doughty *et al.*, 2023; Araújo *et al.*, 2021; Doughty and Goulden, 2008; Kunert *et al.*, 2022; Mau *et al.*, 2018). Although controlled

experiments with ample water availability had shown that the trees could tolerate extreme temperatures via transpirational cooling (Drake *et al.*, 2018), our results of leaf thermoregulation across the 14 leaves of 4 species during the hot and dry period seem to suggest a lack of sufficient cooling during peak leaf temperatures. More studies are necessary to properly understand what the effects of exceedance of thresholds and exposure times would be on the growth and development of the trees ultimately determining the spatial distributions of species, as well as Carbon sequestration and dynamics of tropical forests as a whole. Furthermore, what this means for the agricultural crops of the tropics and strategies on mitigating the future warming should also be addressed.

Chapter 4

Thermal Safety Margins of 55 species under Warming

4.1 Introduction

As global surface temperatures are increasing with time (Hansen *et al.*, 2010), vegetation of the tropics could be at particular risk. Thus, it is important to understand how vulnerable the species of the tropics are to thermal stress. Given the potential impacts of climate change on geographic distributions and species composition (Feeley *et al.*, 2020), identification of species that are relatively more vulnerable to thermal stress would help in conservation activities as well as in afforestation drives to choose species that are more resilient to future warming. As several studies in the tropics have already reported thermal thresholds of photosynthesis (Sastry and Barua, 2017; Slot *et al.*, 2021; O'sullivan *et al.*, 2017), the leaf temperatures, specifically the maximum temperatures, need to be understood in order to calculate thermal safety margins - difference between the maximum leaf temperature and a thermal threshold (Cook *et al.*, 2021) - and assess how safe the species are to thermal stress in current and future climate conditions.

Using air temperature as a proxy for the leaf temperature is not ideal and can lead to erroneous conclusions as leaf temperature tend to be decoupled from air temperatures with the leaf-to-air temperature differences varying drastically across species with recorded differences as high as 12^oC (Fig. 3.7) (Campbell and Norman, 1998; Cook *et al.*, 2021). Leaf temperatures can be measured in the field using thermistors/thermocouples (Chap-

ter 3) (Doughty and Goulden, 2008)), thermal cameras or sensors (Chapter 3), satellite (Doughty *et al.*, 2023), and can also be modeled using leaf energy budget model (Chapter 2) (Kullberg and Feeley, 2022). Leaf Energy Budget model is a mechanism-based approach based on well understood fundamental principles and thus is the tool of choice to predict leaf temperatures of the future. The model uses climatic parameters such as air temperature, relative humidity, and light as well as leaf traits such as effective leaf width, stomatal conductance to solve for leaf temperature (Chapter 2).

Kullberg and Feeley (2022) used a leaf energy budget model to study the thermal safey margins of several tropical and sub-tropical species and showed that the species are well below the thermal thresholds of PSII. Studies such as Miller *et al.* (2021) and Mau *et al.* (2018) have shown that the leaf and, even air temperatures, were exceeding the optimal temperatures of photosynthesis at least in the top-canopy, sun-exposed leaves. Kunert *et al.* (2022) have shown that the temperatures of the Summer were reaching the critical temperatures of photosynthetic decline (T_5 or T_{crit}) and argued that the leaf temperatures, being much higher than air, would be exceeding the thermal thresholds. Alternate ways of calculating safety margins as did by Esperon-Rodriguez *et al.* (2021) and Esperon-Rodriguez *et al.* (2022) using the climate niche of the geographic distributions of several tropical tree species of urban Australia have identified species that could be vulnerable to the changing climate.

The overall objective of the study was to expand on the leaf temperature measurements (Chapter 3) to get thermal safety margins for the 55 species of the tropical forest in the Western Ghats to understand how the vulnerable the forest is to physiological thermal stress. Leaf energy budget model (Chapter 2) was used to estimate maximum leaf temperatures for the Summer of 2023 using climatic parameters measured in the field and taken from global datasets, as well as leaf parameters either measured or taken from literature. Daily maximum air temperatures from CMIP6 - Coupled Model Intercomparison Project 6 - was used to understand how the climate changes in the coming 10 decades and also aid in predicting leaf temperatures of the future under different warming scenarios.

4.2 Methods

Thermal safety margins were estimated for 40 forestry and 15 agroforestry species in the tropical forest in Sirsi, India (Section 3.2). Maximum leaf temperatures were calculated using the leaf energy budget model (Chapter

2) with some additional assumptions as outlined here. Environmental parameters (Table 2.1) were either taken from climate datasets or measured in the field (Fig. 2.3, Section 2.5). Physiological thresholds (Section 3.2) and leaf thermoregulatory traits used in the model were taken from a previous study (Premugh, 2020) and from literature as shown in Table 2.2.

Leaf Energy Budget Model

The model as described in Chapter 2 was used to calculate the maximum leaf temperatures but implemented without incorporating the effect of leaf and solar orientation or rather assuming that the leaves are horizontal, and the dynamic stomatal conductance model. Leaf angles were not included because of unavailability of the data for the 55 species. And for stomatal conductance, it tend to be near zero during times of extreme temperatures. Given we are only interested in the maximum leaf temperatures and that the species differences in stomatal condutance might not matter at very low conductances (Section 2.7), we used a constant value of 0.01 $\mu\ mols\ m^{-2}s^{-1}$ for all the species which is a conservative estimate assuming a reduction of stomatal conductance to 10% of the maximal stomatal conductance ($\sim 0.1\ \mu\ mols\ m^{-2}s^{-1}$)

For the summer, maximum leaf temperature for each day was estimated by modeling leaf temperatures between $1PM$ and $3PM$. All the necessary parameters were as defined in the tables 2.1, 2.2, and 2.3. The net radiation was estimated using the equation 2.3 where R_s is the global solar radiation estimated from the field measurements of PAR (Fig. 2.3). The leaf energy balance (Eq. 2.2) were then solved using the rest of the fluxes and parameters defined in Sections 2.2 and 2.5 assuming a constant g_s ($0.01\ \mu\ mols\ m^{-2}s^{-1}$).

Validating the Model

Validation of the dynamic model with the angles and stomatal conductance model is discussed in section 2.6. The version of the model used here was validated using the daily maximum leaf temperatures from the high-resolution, long-term leaf temperature measurements (Figs. 3.5, 3.6) by estimating leaf temperatures assuming horizontal leaves and constant stomatal conductance. For each day from the long-term time series, maximum leaf temperature was modeled at times when the leaf hits the maximum temperature. During each time step, a Monte-Carlo approach was taken by repeating the modeling process at each time step by randomly sampling

from the distributions of wind, cloudcover, and effective leaf width to get a confidence around each data as explained in the section 2.7. The standard deviations are added as an error bar in the scatters comparing the modeled and the measured leaf tempratures for the 14 traces (Fig. 4.1).

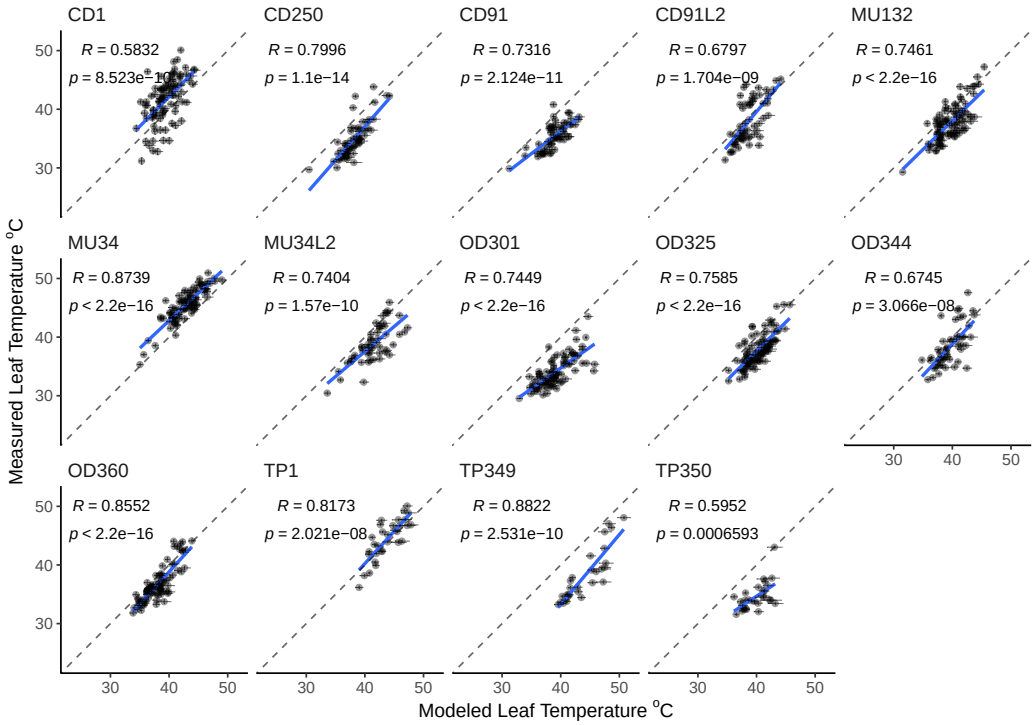

Figure 4.1: **Comparison of modeled and measured daily maximum leaf temperatures** for leaves of the 4 focal forestry species (Table 3.1). The error bars along the x and y axes represent the Monte-Carlo Uncertainty estimated by random sampling of parameters. Dashed line represents equality. CD: *Canthium*, MU: *Memecylon*, OD: *Olea*, and TP: *Terminalia*.

In general, there seems to be a slight overestimation of maximum leaf temperatures by 1 to 2 ^oC. For two leaves of *Terminalia*, the difference is as high as 3 to 5^oC. The absence of a better agreement could be attributable to the lack of confidence in the wind and cloudcover data from ERA5 particulary at the time scale that we are working with given how sensitive the model predictions are to the two parameters (Section 2.7) and the mismatch between the measured PARs and what the leaves actually see (Section 2.6). The leaves TP1 and OD360 have the best agreement between the modeled and the predicted where as leaves like CD1 and OD301

didn't have PAR sensors that could capture the microtopographical variations in light levels.

Future Climate - CMIP6 & ERA5

To predict leaf temperatures of the future and infer the vulnerability of the 55 species, we used climate projections from CMIP6 - Coupled Model Intercomparison Project 6 - which coordinates different experiments and simulations of future climate run by different organizations around the world. For this study, models that followed conditions set by Scenario MIP was used. Out of experiments that define a set of forcing parameters - emissions and socioeconomic assumptions - called the SPPs or Shared Socioeconoic Pathways, SSP126, SSP245 and SSP585 were chosen as they represent a low, medium and high forcing scenarios respectively (O'Neill *et al.*, 2016). SSP126 assumes a a sustainable society with a climate forcing of $2.6Wm^{-2}$ in 2100. Whereas SSP245 assumes a world with regional rivalries and $4.5Wm^{-}2$ forcing and SSP585 a completey fossil based society with $8.5Wm^{-2}$ of forcing in 2100.

Although daily maximum air temperature (tasmax), near-surface relative humidity (hurs), downwelling thermal radiation (rlds), and upwelling thermal radiation (rlus) at a daily scale were availabe from CMIP6, we could not use the data to directly predict the leaf temperatures. This was because the daily maximum air temperature - tasmax - from CMIP6 for our site did not correlate well with the air temperatures measured at the site during the Summer of 2023 (Fig. A.3). Across the three scenarios, tasmax ranged between 32^oC and 36^oC in 2023, while the measured data varied between 32^oC and 42^oC with the means of the two datasets differing by 2.5^oC and the maximums by 4^oC. Thus, to predict leaf temperatures of 2100, current air temperatures measured at the site was translated by the change in the mean tasmax air temperatures under the moderate scenario (SSP245 - 1.7^oC) and the extreme scenario (SSP585 - 3.9^oC). Parameters such as wind, solar radiation and relative humidity would not change considerably in the future and the CMIP6 predictions for these parameters do not show in changes until 2100. But the upwelling and the downwelling thermal radiation do change with time at different rates across the scenarios. Though the change in air temperature would capture the increases in downwelling thermal radiation (Section 2.2) to some extend, the increase in upwelling thermal radiation won't be accounted for in the current implemenation of the model. The impact of such would probably be that the leaf temperatures of the future would thus likely be slightly underestimated.

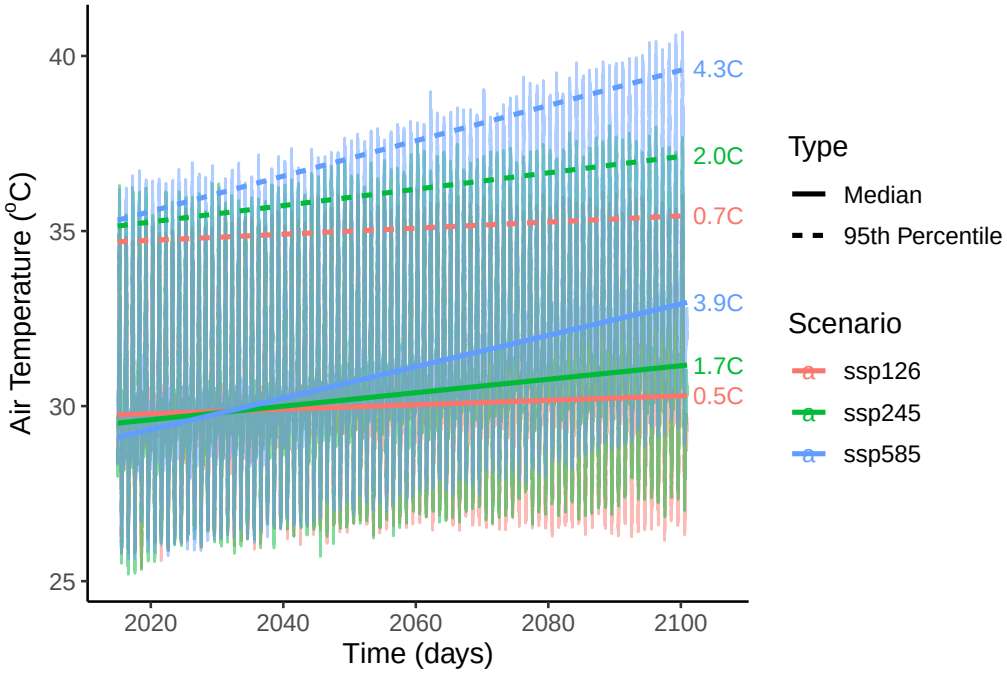

Figure 4.2: **Daily maximum air temperatures at the surface - tasmax - from CMIP6 for three scenarios.** SSP126 (red) represents a highly optimistic future with the least amount of warming, while SSP585 (blue) was the worst case scenario and SSP245, a medium level warming. The straight and the dashed lines are linear and quantile (95^{th} percentile) regressions. The change in temperatures between the beginning and 2100 is shown on the right side of the plots near the lines. The spread of the predictions from different models and their sources are given in Fig. A.4

.

4.3 Results

4.3.1 Maximum leaf temperatures and TSMs of the 55 species

Daily maximum leaf temperatures were modeled for the 55 species for the summer of 2023 (Fig. 4.3). There were several days throughout the three months that the leaf temperatures have crossed into the range of T_{50}s. Towards the end of April and beginning of May have the highest incidences of leaf temperatures exceeding T_{50}s as these were the hottest and driest periods of the season (Fig. 2.3). The daily 95^{th} percentile leaf temperatures varied from 38^oC to as high 49^oC while the T_{50}s ranged between 46^oC and

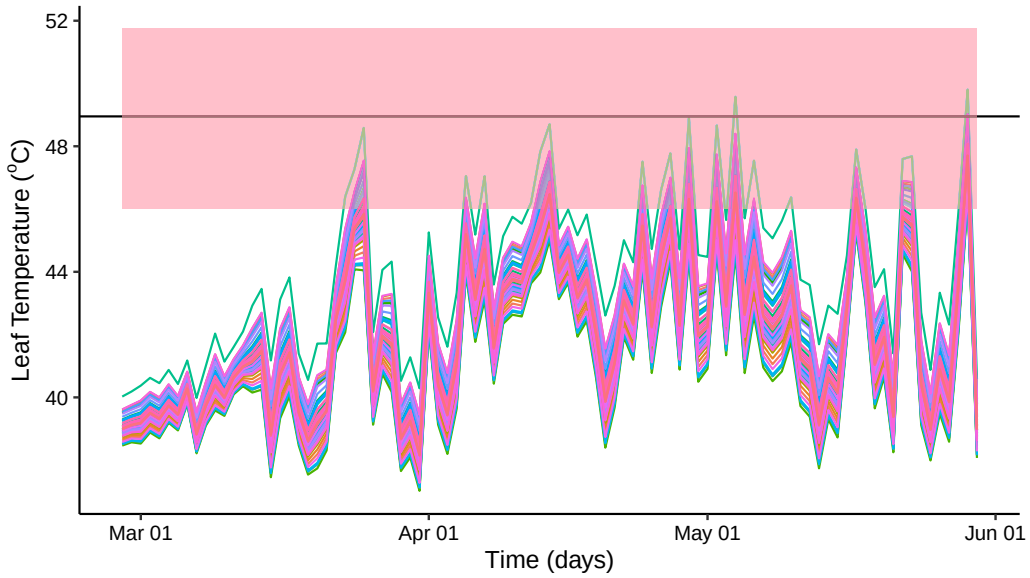

Figure 4.3: **Model predictions of daily 95^{th} percentile leaf temperatures.** Different colors represent the 55 species. Pink rectangular region shows the range of T_{50}s.

51.8^oC, and T_5s between 40.3^oC and 47.7^oC (Fig. 4.3, Table 4.1). At the temporal scale of the current modeling framework, estimating the continuous time of exposure above the physiological threshold is unfeasable.

Distributions of the top 5 percentile model predicted leaf temperatures across the 3 months for the 55 species are shown in Fig. 4.4. 95^{th} percentile leaf temperatures varied between 43^oC for Clove to 46.4^oC for *Macarenga peltata* while maximums varied from 46.6^oC to 50^oC. Currently, the extreme temperatures of most of the species are well above their T_5s and below their T_{50}s. For 24 species, the top 5 percentile leaf temperatures were atleast half a degree above their T_5s. 12 species were exceeding their T_{50}s and for *Cocoa*, *Careya arboria*, *Pepper*, *Stereospermum personatum*, and *Macarenga peltata* have more than 25% of the extreme temperatures (Fig. 4.4) falling above their T_{50}s with thermal safety margins, difference between T_{50}s and 95^{th} percentile leaf temperatures, were -3^oC, -1.8^oC, -1.2^oC, 1.0^oC and 1.1^oC respectively.

Comparisons between the estimated leaf temperatures with T_5s, T_{50}s and $TSMs$ are shown in Fig. 4.5. The maximum leaf tempertures show no significant correlations with both T_{50}s (r = -0.16, p = 0.23) and T_5s (r = 0.036, p = 0.8). Looking at correlations between the maximum leaf tem-

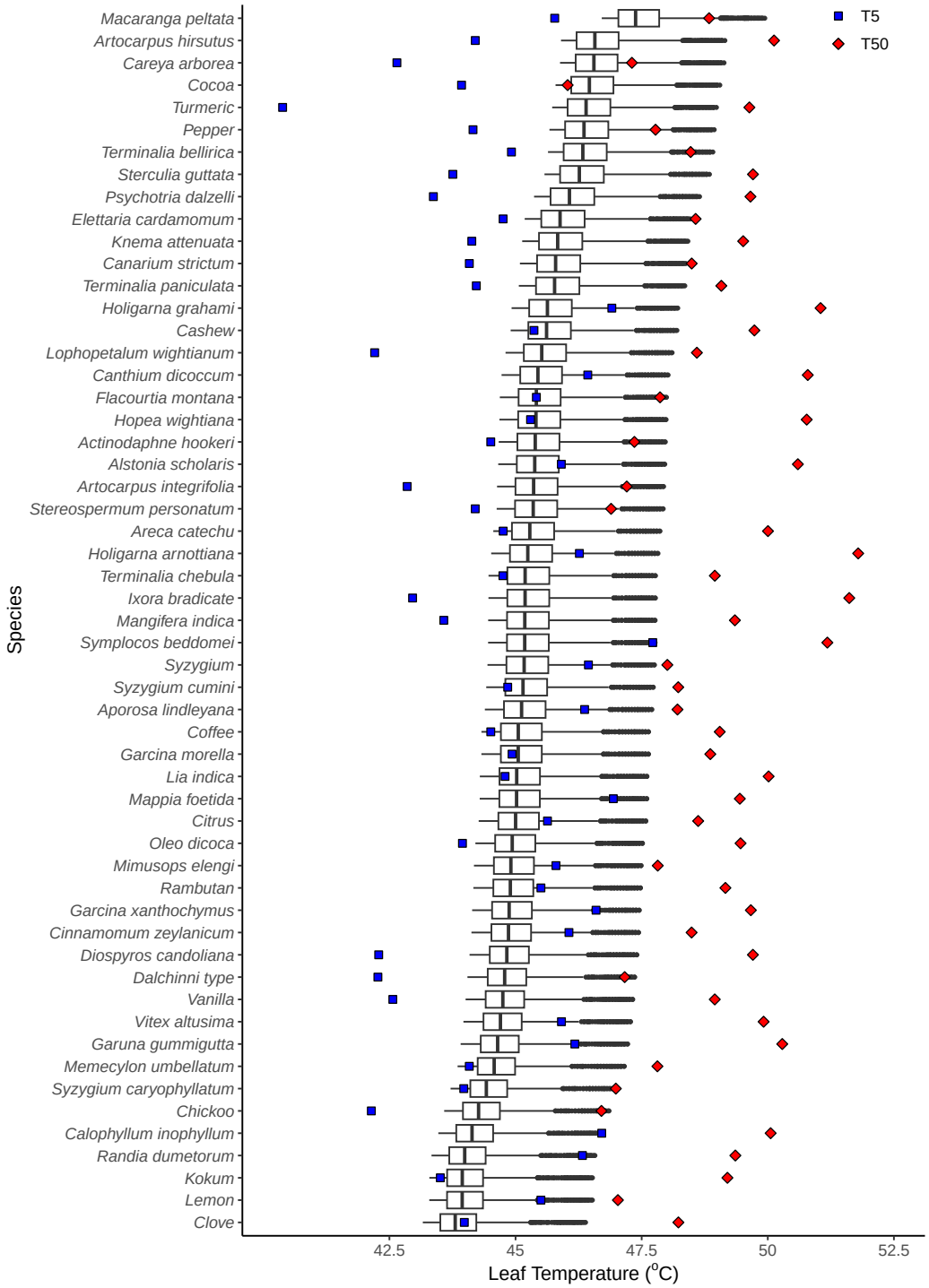

Figure 4.4: **Distributions of top 5 percentile model predicted leaf temperatures and photosynthetic thresholds.** Blue squares are T_5s and red diamonds are T_{50}s.

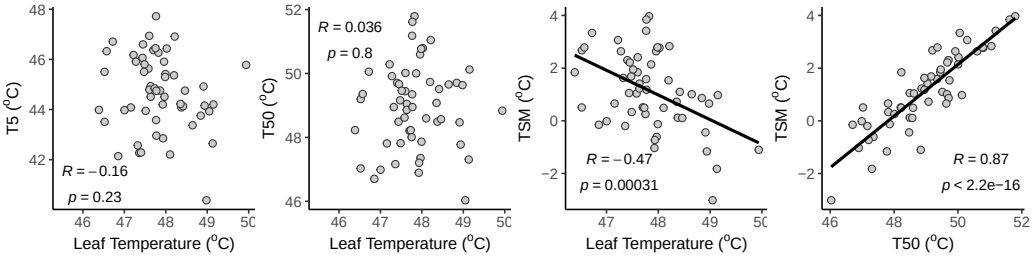

Figure 4.5: **Correlations between the estimated maximum leaf temperatures, T_5s, T_{50}s, and TSMs.** Pearson's r and p-value are given as insets and regression lines are shown for significant correlations.

peratures with TSMs and T_{50}s needs particular attention when making conclusions as the TSMs were essentially calculated from the other two variables. TSMs showed a strong negative correlation with the maximum leaf temperature (r = -0.47, p $<$ 0.05) and a strong positive correlation with T_{50}s (r = 0.87, p $<$ 87). Thus, it can be said that, in general, species that experienced more extreme temperatures tend to show low thermal safety margins and so were the species with low thermotolerance or T_{50}s.

4.3.2 Future predictions of exposures and TSMs

Leaf temperatures were predicted for the year 2100 assuming an increase in air temperature of 1.7^oC and 3.9^oC based on CMIP6 predictions for the region (Fig. 4.2). At 1.7^oC increase in air temperature, the range of 95^{th} percentile leaf temperatures varied between 45^oC to 51^oC where as for 3.9^C warming, the range of the percetiles were 47^oC to 52.5^oC. The range of T_5s, 40.3^oC and 47.7^oC, were already below the range of extreme leaf temperatures. For the moderate warming scenario where the TSMs ranged between 2.1^oC and -4.3^oC, the number of species with a positive safety margin dropped from the current 44 species to 24, and for the worst case scenario where the range of TSMs shifted to 0.4^oC to -5.9^oC, the number was mere 4 species.

The percentage of days when the daily maximum leaf temperature exceeded either T_5s and T_{50}s are shown in Fig. 4.6). Exceedence of T_5s do not necessarily lead to higher exceedence of T_{50}s. Under current climate, *Turmeric*, *Careya arborea* and *Lophopetalum wightianum* are the three species with the highest percentage of days with leaf temperatures exceeding T_5s - 86%, 58.1%, and 50.5% respectively. Where 3 species out of the 55 had more than 50% of days with exposure to T_5s, the model predicted 14 species in 2100 under the moderate scenario and 37 species under the

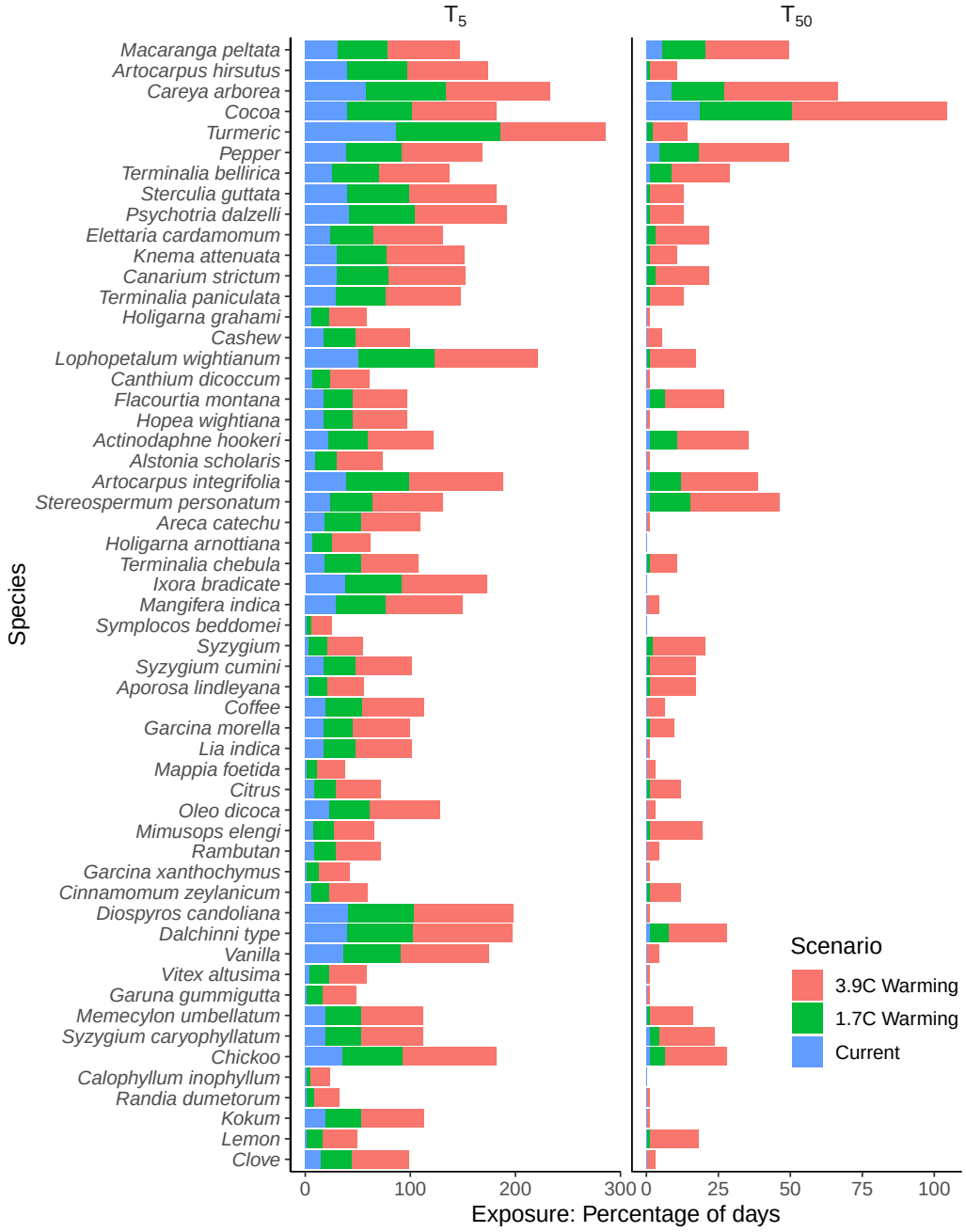

Figure 4.6: **Percentage of days when the daily maximum leaf temperature exceeded T_5 (left) and T_{50} (right)** under different warming scenarios. Blue is from the leaf temperatures modeled for the current time (Fig. 4.4) where as green and red are from the leaf temperatures modeled for the Summer of 2100 assuming an increase of 1.7^oC and 3.9^oC in the air temperatures (Fig. 4.2).

worst case. With respect to T_{50}s, *Cocoa*, *Careya arboea* and *Macarenga peltata* had the highest exposures under the current climatic conditions - 18.3%, 8.6% and 5.4% respectively. Whereas 12 species had atleast a day with exposure to T_{50}s in recent times, the number could increase in the future to 34 and 51 species under 1.7^oC and 3.9^oC warming scenarios respectively.

4.4 Discussion

Leaf energy budget model was used to get estimates of maximum leaf temperatures for the Summer of 2023 for the 55 forestry and agroforestry species. The species-specificity in leaf temperatures was purely captured by the variation in effective leaf width. Other leaf thermoregulatory parameters such as stomatal conductance and leaf angles were not taken as different for the species in calculation of the maximum leaf temperatures. The estimates of maximum leaf temperatures differed within 4^oC to 5^oC across species. The range of variation in the physiological thresholds - T_5s and T_{50}s - are also in the order of 5^oC. The results did not show any correlations between the extreme leaf temperatures experienced and the measures of thermotolerance (Fig. 4.5). In other words, species with the warmest leaves were not necessarily the most thermotolerant. As such, it cannot be assumed that the most thermotolerant species are relatively safer against thermal stress and it also shows the necessity to have measures or estimates of leaf temperatures to put physiological thresholds in perspective.

The study was able to identify species that might relatively be more vulnerable to thermal stress. *Cocoa*, *Macarenga peltata*, *Careya arborea*, *Pepper*, *Turmeric*, and *Artocarpus hirsutus* are a few of the species that are likely to be at greater risks of declining photosynthesis and potentially irreversible damages to leaf machineries that govern the plant physiology and, at worse cases, even leaf lethality. The results are insufficient to make comments on the impacts the leaves of the 55 species would have endured during the study period as it could not estimate the continuous time of exposure above the physiological thresholds. To get the continuous time of exposure or the duration of uniterrupted exposure, we'd need leaf temperatures at higher resolution ($1min$ or so) for longer periods of time. As the physiological thresholds used in the study were from 30 minutes thermotolerance assays (Premugh, 2020), leaves would probably need to experience 30 minutes of exposures above T_{50} to sustain irreversible damages. But, what the current study was trying to achieve was to discern species that

could potentially be experiencing or likely to be subjected to experience in the future, scenarios of exposures that can lead to thermal stress and eventually damages and leaf lethality. As the global surface temperatures rise and extreme weather events like heatwaves increase in intensity, duration and frequency (Rahmstorf *et al.*, 2017; Trenberth, 2011), the species with the lowest thermal safety margins, essentially the ones whose leaf temperatures were already exceeding T_{50}s, would likely be the ones to increasingly experience damage-inducing and lethal exposures.

The primary objective of the study was to assess the vulnerability of a tropical forest to physiological thermal stress in the Western Ghats under current and future climate conditions. As relatively vulnerable species are identified, more needs to be done to better understand, particularly, the impact of exceedence of the thresholds and what it means for the future distributions of the species. Vulnerabilities and thus impacts need to be distinguished between species like *Turmeric* with a large difference of approximately 9.3^oC between T_{50} and T_5 as opposed to *Syzygium* with a difference of 2.6^oC. Although the study was able to demonstrate one of the major applications of the leaf energy budget model, it comes with several caveats such as the exclusion of species-specific maximal stomatal conductance and leaf orientations, and the inability to estimate continuous exposure times under the current framework.

Table 4.1: **T_{50}s, percentage of days exceeding T_{50}s and T_5s, and thermal safety margins of the 55 species under future warming.** Exposures and TSMs are given for the current climate conditions and two warming scenarios - SSP245 with 1.7^oC increase in air temperature in 2100, and SSP585 with 3.9^oC.

Species	T_{50}	Exposure $T_{leaf} > T_5$	Exposure $T_{leaf} > T_{50}$	TSM
		0/1.7/3.9	0/1.7/3.9	0/1.7/3.9
	^oC	%	%	^oC
Cocoa	46.0 ± 1.9	39.8/61.3/80.6	18.3/32.3/53.8	-3/-4.3/-5.9
Careya arborea	47.3 ± 1.0	58.1/75.3/100	8.6/18.3/39.8	-1.8/-3.1/-4.7
Pepper	47.8 ± 1.4	38.7/52.7/77.4	4.3/14/31.2	-1.2/-2.4/-4
Stereospermum personatum	46.9 ± 2.3	23.7/39.8/67.7	1.1/14/31.2	-1/-2.3/-4
Macaranga peltata	48.8 ± 1.3	31.2/47.3/68.8	5.4/15.1/29	-1.1/-2.3/-3.9
Artocarpus integrifolia	47.2 ± 1.9	38.7/60.2/89.2	1.1/10.8/26.9	-0.7/-2/-3.7
Actinodaphne hookeri	47.4 ± 0.9	21.5/37.6/63.4	1.1/9.7/24.7	-0.6/-1.9/-3.6
Chickoo	46.7 ± 1.8	35.5/57/89.2	1.1/5.4/21.5	-0.2/-1.5/-3.3
Dalchinni type	47.2 ± 1.5	39.8/62.4/94.6	1.1/6.5/20.4	-0.2/-1.5/-3.3
Flacourtia montana	47.9 ± 1.7	17.2/28/51.6	1.1/5.4/20.4	-0.1/-1.4/-3.1
Terminalia bellirica	48.5 ± 0.6	25.8/44.1/67.7	1.1/7.5/20.4	-0.4/-1.7/-3.3
Syzygium caryophyllatum	47.0 ± 1.2	19.4/33.3/59.1	1.1/3.2/19.4	0/-1.4/-3.1
Canarium strictum	48.5 ± 1.5	30.1/48.4/74.2	0/3.2/18.3	0.1/-1.2/-2.8
Elettaria cardamomum	48.6 ± 0.7	23.7/40.9/66.7	0/3.2/18.3	0.1/-1.2/-2.8
Mimusops elengi	47.8 ± 1.2	7.5/19.4/38.7	0/1.1/18.3	0.3/-1/-2.7
Syzygium	48.0 ± 1.3	3.2/17.2/34.4	0/2.2/18.3	0.3/-1.1/-2.8
Lemon	47.0 ± 0.9	1.1/15.1/33.3	0/1.1/17.2	0.5/-0.9/-2.7
Aporosa lindleyana	48.2 ± 1.1	3.2/17.2/35.5	0/1.1/16.1	0.5/-0.8/-2.5
Lophopetalum wightianum	48.6 ± 1.6	50.5/72/98.9	0/1.1/16.1	0.5/-0.8/-2.5
Syzygium cumini	48.2 ± 1.2	17.2/30.1/53.8	0/1.1/16.1	0.5/-0.8/-2.5
Memecylon umbellatum	47.8 ± 1.3	19.4/33.3/59.1	0/1.1/15.1	0.7/-0.7/-2.5
Psychotria dalzelli	49.7 ± 1.3	41.9/62.4/87.1	0/1.1/11.8	1/-0.3/-1.9
Sterculia guttata	49.7 ± 1.3	39.8/59.1/82.8	0/1.1/11.8	0.9/-0.4/-2
Terminalia paniculata	49.1 ± 2.1	29/47.3/72	0/1.1/11.8	0.7/-0.6/-2.2
Turmeric	49.6 ± 1.5	86/100/100	0/2.2/11.8	0.7/-0.6/-2.2
Cinnamomum zeylanicum	48.5 ± 1.7	5.4/17.2/36.6	0/1.1/10.8	1.1/-0.3/-2
Citrus	48.6 ± 2.3	8.6/20.4/43	0/1.1/10.8	1/-0.3/-2

Table continued in next page

Artocarpus hirsutus	50.1 ± 2.7	39.8/57/77.4	0/1.1/9.7	1/-0.3/-1.9
Knema attenuata	49.5 ± 1.4	30.1/47.3/74.2	0/1.1/9.7	1.1/-0.2/-1.9
Terminalia chebula	48.9 ± 1.2	18.3/34.4/54.8	0/1.1/9.7	1.2/-0.1/-1.9
Garcina morella	48.9 ± 0.8	17.2/28/53.8	0/1.1/8.6	1.2/-0.1/-1.8
Coffee	49.0 ± 1.2	19.4/34.4/59.1	0/0/6.5	1.4/0.1/-1.6
Cashew	49.7 ± 1.7	17.2/30.1/52.7	0/0/5.4	1.5/0.2/-1.4
Mangifera indica	49.3 ± 2.4	29/47.3/73.1	0/0/4.3	1.6/0.3/-1.5
Rambutan	49.2 ± 1.5	8.6/20.4/43	0/0/4.3	1.7/0.3/-1.4
Vanilla	48.9 ± 1.4	36.6/53.8/84.9	0/0/4.3	1.6/0.3/-1.5
Clove	48.2 ± 1.9	15.1/29/54.8	0/0/3.2	1.8/0.5/-1.3
Mappia foetida	49.4 ± 0.8	1.1/9.7/26.9	0/0/3.2	1.8/0.5/-1.2
Oleo dicoca	49.5 ± 1.3	22.6/38.7/66.7	0/0/3.2	1.9/0.6/-1.1
Alstonia scholaris	50.6 ± 1.2	9.7/20.4/43	0/0/1.1	2.6/1.3/-0.4
Areca catechu	50.0 ± 1.7	18.3/34.4/57	0/0/1.1	2.1/0.8/-0.9
Canthium dicoccum	50.8 ± 2.3	6.5/17.2/37.6	0/0/1.1	2.8/1.5/-0.2
Diospyros candoliana	49.7 ± 1.6	40.9/62.4/94.6	0/0/1.1	2.3/1/-0.8
Garcina xanthochymus	49.7 ± 2.0	1.1/11.8/29	0/0/1.1	2.2/0.9/-0.9
Garuna gummigutta	50.3 ± 1.4	1.1/15.1/32.3	0/0/1.1	3.1/1.7/0
Holigarna grahami	51.0 ± 1.0	5.4/17.2/35.5	0/0/1.1	2.8/1.5/-0.1
Hopea wightiana	50.8 ± 2.4	17.2/28/51.6	0/0/1.1	2.8/1.5/-0.2
Kokum	49.2 ± 1.3	19.4/33.3/60.2	0/0/1.1	2.7/1.3/-0.5
Lia indica	50.0 ± 1.3	17.2/30.1/53.8	0/0/1.1	2.4/1.1/-0.6
Randia dumetorum	49.4 ± 0.8	1.1/7.5/23.7	0/0/1.1	2.8/1.4/-0.4
Vitex altusima	49.9 ± 1.1	4.3/18.3/35.5	0/0/1.1	2.6/1.3/-0.5
Calophyllum inophyllum	50.1 ± 2.5	1.1/3.2/19.4	0/0/0	3.3/2/0.2
Holigarna arnottiana	51.8 ± 1.6	6.5/18.3/37.6	0/0/0	4/2.6/0.9
Ixora bradicate	51.6 ± 1.9	37.6/53.8/81.7	0/0/0	3.8/2.5/0.8
Symplocos beddomei	51.2 ± 1.6	1.1/4.3/20.4	0/0/0	3.4/2.1/0.4

Chapter 5

Conclusions

Air temperatures in the tropical forest in Western Ghats are predicted to increase by 2^oC to 4^oC in 2100 (Fig. 4.2) as with the climate change in the tropical forests around the world (Williams *et al.*, 2003), and the overall global warming (Rahmstorf *et al.*, 2017) and changes in precipitation regimes and extreme weather events (Trenberth, 2011). Thus, the increase in leaf temperatures, which would influence the physiological processes of plants, would have serious implications on the dynamics of these forests. The crux of the study was then to understand the leaf temperatures experienced by multiple species of a tropical forest in the Western Ghats, to assess potential heat-induced damages and put the physiological thresholds of CO_2 assimilation and Photosystem II quantum yield into perspective. Long-term leaf temperatures at high temporal resolution for 4 forestry species and maximum leaf temperatures during the hottest and driest period of the season for 13 agroforestry species were measured. Fv/Fms of Sun-exposed and shade leaves were then probed to capture potentially heat-induced declines in the PSII quantum efficiency, as well as a qualitative analysis of leaf necrosis. To further build on the leaf temperatures and physiological thresholds of a few species, leaf energy budget model was implemented and applied to get estimates of maximum leaf temperatures for 55 species under current and future climate conditions.

The high-resolution, long-term leaf temperature data is one of the only datasets reported so far that were able to capture continuous variations of leaf temperature through the summer for multiple leaves of 4 species. In addition to the strong observed diurnal and seasonal patterns (Figs. 3.5, 3.6, 3.7), leaves consistenty exceeded physiological thresholds of CO_2 assimilation potentially spending hours with less optimal rates of photosyn-

thesis, as well as occassionally approaching thresholds of PSII quantum yield. The observed ranges of continuous exposure times above T_5s and T_{50}s across the 14 leaves are not sufficient to suggest that they could be enduring irreversible damages, generally associated with exposures above T_{50}s (Sastry and Barua, 2017), to leaf machineries responsible for the physiological processes such as photosynthesis and respiration. A steadily warming world could lead to increase in the extreme leaf temperatures and the exposure times possibly to levels that can lead to irreversible damages and eventually to leaf lethality.

The Fv/Fm measurements taken to assess the impacts are suggestive of potentially heat-induced damages to PSII as species with the highest percentage of leaves exceeding the thresholds showed significant declines in PSII quantum efficiency (Figs. 3.10, 3.11). In addition to the consistently lower Fv/Fm values of Sun-exposed leaves as compared to the shade leaves across the probed species, the measurements showed large variation for three agriculturally important species - *Cocoa*, *Cinnamon* and *Vanilla* indicating reduced photosynthetic output. For these species, the continuous exposure times were unknown, but the 4 species, for which we have the long-term data, do not show concerning levels of declines. Further, the thermal safety margins, estimated using the leaf energy budget model, predicted that the number of species with exceedance of T_{50} could increase to 34 to 51 species in the future depending on the amount of warming. Although the exposure times of these identified vulnerable species are unknown, it is likely that the rise in temperatures and increase in intensity and durations of events like heatwaves, would lead to harmful exposure times for these species. Further work is required to understand the effects of exceedence and exposures times of leaf temperatures above the thresholds on the physiological processes and ultimately the growth and development of the plants.

Although there are arguments of leaves being able to regulate their temperatures below that of air (Michaletz *et al.*, 2016; Kullberg and Feeley, 2022) and controlled experiments had suggested that the trees would be able to transpirationally cool and cope through extreme events like heatwaves (Drake *et al.*, 2018), the patterns of leaf-to-air temperature differences that were recorded through the summer do not seem to show that the cooling would be sufficient to adequately lower leaf temperatures, particularly during peak solar hours. As such, it is unlikely that under future warming, that the leaves would be able to mitigate the changes and keep the exposure times above the thresholds below harmful and lethal levels. A detailed sensitivity analysis can help here in understanding the

major drivers of leaf temperatures and to ask why leaves are unable to regulate extreme temperatures. Another aspect of vulnerability that was not considered in the study are the acclimation of physiological thresholds (Choury *et al.*, 2022) and leaf thermoregulatory traits (Kullberg and Feeley, 2022; Kullberg *et al.*, 2023) in response to rising temperatures. Though further works are required to properly address questions regarding acclimation of thresholds and parameters, what we know so far do not seem to suggest that the acclimation rates would be sufficient to compensate for the predicted changes in temperatures.

The overall results suggest that the tropical forest of Western Ghats are vulnerable to physiological thermal stress and evidences for a few species are indicative of prevailing heat-induced damages. This study adds on to several recent studies from the tropical forests around the world reporting that the leaf temperatures are approaching and exceeding physiological thresholds (Doughty *et al.*, 2023; Araújo *et al.*, 2021; Doughty and Goulden, 2008; Kunert *et al.*, 2022; Mau *et al.*, 2018). This strongly suggests the necessity of having long-term leaf temperature data like the ones that we reported here and still more needs to be done to properly report the impacts of exceedences of thresholds and exposure times. Further works are required to understand how much the trees would be able to acclimate to alleviate the effects of extreme temperatures.

References

Antonanzas-Torres F, Urraca R, Polo J, Perpiñán-Lamigueiro O, Escobar R (2019). Clear sky solar irradiance models: A review of seventy models. Renewable and Sustainable Energy Reviews 107, 374–387.

Araújo I, Marimon BS, Scalon MC, Fauset S, Marimon Junior BH, Tiwari R, Galbraith DR, Gloor MU (2021). Trees at the Amazonia-Cerrado transition are approaching high temperature thresholds. Environmental Research Letters 16(3), 034047.

Aubrecht DM, Helliker BR, Goulden ML, Roberts DA, Still CJ, Richardson AD (2016). Continuous, long-term, high-frequency thermal imaging of vegetation: Uncertainties and recommended best practices. Agricultural and Forest Meteorology 228–229, 315–326.

Ball JT, Woodrow IE, Berry JA (1987). A Model Predicting Stomatal Conductance and its Contribution to the Control of Photosynthesis under Different Environmental Conditions. In J Biggins, editor, Progress in Photosynthesis Research, 221–224. Springer Netherlands, Dordrecht.

Berry J, Bjorkman O (1980). Photosynthetic Response and Adaptation to Temperature in Higher Plants. Annual Review of Plant Physiology 31(1), 491–543.

Bonan GB (2016). Ecological Climatology: Concepts and Applications. Cambridge University Press, New York, NY, USA, third edition edition.

Bonan GB, Williams M, Fisher RA, Oleson KW (2014). Modeling stomatal conductance in the earth system: Linking leaf water-use efficiency and water transport along the soil–plant–atmosphere continuum. Geoscientific Model Development 7(5), 2193–2222.

Brienen RJW, Phillips OL, Feldpausch TR, Gloor E, Baker TR, Lloyd J, Lopez-Gonzalez G, Monteagudo-Mendoza A, Malhi Y, Lewis SL,

Vásquez Martinez R, Alexiades M, Álvarez Dávila E, Alvarez-Loayza P, Andrade A, Aragão LEOC, Araujo-Murakami A, Arets EJMM, Arroyo L, Aymard C GA, Bánki OS, Baraloto C, Barroso J, Bonal D, Boot RGA, Camargo JLC, Castilho CV, Chama V, Chao KJ, Chave J, Comiskey JA, Cornejo Valverde F, da Costa L, de Oliveira EA, Di Fiore A, Erwin TL, Fauset S, Forsthofer M, Galbraith DR, Grahame ES, Groot N, Hérault B, Higuchi N, Honorio Coronado EN, Keeling H, Killeen TJ, Laurance WF, Laurance S, Licona J, Magnussen WE, Marimon BS, Marimon-Junior BH, Mendoza C, Neill DA, Nogueira EM, Núñez P, Pallqui Camacho NC, Parada A, Pardo-Molina G, Peacock J, Peña-Claros M, Pickavance GC, Pitman NCA, Poorter L, Prieto A, Quesada CA, Ramírez F, Ramírez-Angulo H, Restrepo Z, Roopsind A, Rudas A, Salomão RP, Schwarz M, Silva N, Silva-Espejo JE, Silveira M, Stropp J, Talbot J, ter Steege H, Teran-Aguilar J, Terborgh J, Thomas-Caesar R, Toledo M, Torello-Raventos M, Umetsu RK, van der Heijden GMF, van der Hout P, Guimarães Vieira IC, Vieira SA, Vilanova E, Vos VA, Zagt RJ (2015). Long-term decline of the Amazon carbon sink. Nature 519(7543), 344–348.

Campbell GS, Norman JM (1998). Introduction to Environmental Biophysics. Springer, New York, 2nd ed edition.

Carmona F, Rivas R, Caselles V (2014). Estimation of daytime downward longwave radiation under clear and cloudy skies conditions over a subhumid region. Theoretical and Applied Climatology 115(1-2), 281–295.

Choury Z, Wujeska-Klause A, Bourne A, Bown NP, Tjoelker MG, Medlyn BE, Crous KY (2022). Tropical rainforest species have larger increases in temperature optima with warming than warm-temperate rainforest trees. New Phytologist 234(4), 1220–1236.

Cook AM, Berry N, Milner KV, Leigh A (2021). Water availability influences thermal safety margins for leaves. Functional Ecology 35(10), 2179–2189.

Damour G, Simonneau T, Cochard H, Urban L (2010). An overview of models of stomatal conductance at the leaf level: Models of stomatal conductance. Plant, Cell & Environment no–no.

Deutsch CA, Tewksbury JJ, Huey RB, Sheldon KS, Ghalambor CK, Haak DC, Martin PR (2008). Impacts of climate warming on terrestrial ectotherms across latitude. Proceedings of the National Academy of Sciences 105(18), 6668–6672.

Dong N, Prentice IC, Harrison SP, Song QH, Zhang YP (2017). Biophysical homoeostasis of leaf temperature: A neglected process for vegetation and land-surface modelling. Global Ecology and Biogeography 26(9), 998–1007.

Doughty CE, Goulden ML (2008). Are tropical forests near a high temperature threshold? Journal of Geophysical Research: Biogeosciences 113(G1).

Doughty CE, Keany JM, Wiebe BC, Rey-Sanchez C, Carter KR, Middleby KB, Cheesman AW, Goulden ML, da Rocha HR, Miller SD, Malhi Y, Fauset S, Gloor E, Slot M, Oliveras Menor I, Crous KY, Goldsmith GR, Fisher JB (2023). Tropical forests are approaching critical temperature thresholds. Nature 1–7.

Doughty CE, Santos-Andrade PE, Shenkin A, Goldsmith GR, Bentley LP, Blonder B, Díaz S, Salinas N, Enquist BJ, Martin RE, Asner GP, Malhi Y (2018). Tropical forest leaves may darken in response to climate change. Nature Ecology & Evolution 2(12), 1918–1924.

Drake JE, Tjoelker MG, Vårhammar A, Medlyn BE, Reich PB, Leigh A, Pfautsch S, Blackman CJ, López R, Aspinwall MJ, Crous KY, Duursma RA, Kumarathunge D, De Kauwe MG, Jiang M, Nicotra AB, Tissue DT, Choat B, Atkin OK, Barton CVM (2018). Trees tolerate an extreme heatwave via sustained transpirational cooling and increased leaf thermal tolerance. Global Change Biology 24(6), 2390–2402.

Esperon-Rodriguez M, Baumgartner JB, Beaumont LJ, Lenoir J, Nipperess D, Power SA, Richard B, Rymer PD, Tjoelker MG, Gallagher RV (2021). Climate-change risk analysis for global urban forests. Preprint, Ecology.

Esperon-Rodriguez M, Rymer PD, Power SA, Barton DN, Cariñanos P, Dobbs C, Eleuterio AA, Escobedo FJ, Hauer R, Hermy M, Jahani A, Onyekwelu JC, Östberg J, Pataki D, Randrup TB, Rasmussen T, Roman LA, Russo A, Shackleton C, Solfjeld I, van Doorn NS, Wells MJ, Wiström B, Yan P, Yang J, Tjoelker MG (2022). Assessing climate risk to support urban forests in a changing climate. PLANTS, PEOPLE, PLANET 4(3), 201–213.

Farquhar GD, von Caemmerer S, Berry JA (1980). A biochemical model of photosynthetic CO2 assimilation in leaves of C3 species. Planta 149(1), 78–90.

Fauset S, Freitas HC, Galbraith DR, Sullivan MJ, Aidar MP, Joly CA, Phillips OL, Vieira SA, Gloor MU (2018). Differences in leaf thermoregulation and water use strategies between three co-occurring Atlantic forest tree species: Leaf energy balance of Atlantic forest trees. Plant, Cell & Environment 41(7), 1618–1631.

Feeley K, Martinez-Villa J, Perez T, Silva Duque A, Triviño Gonzalez D, Duque A (2020). The Thermal Tolerances, Distributions, and Performances of Tropical Montane Tree Species. Frontiers in Forests and Global Change 3.

Fleagle RG, Businger JA (1980). An Introduction to Atmospheric Physics. Number v. 25 in International Geophysics Series. Academic Press, New York, 2d ed edition.

Grose MR, Narsey S, Delage FP, Dowdy AJ, Bador M, Boschat G, Chung C, Kajtar JB, Rauniyar S, Freund MB, Lyu K, Rashid H, Zhang X, Wales S, Trenham C, Holbrook NJ, Cowan T, Alexander L, Arblaster JM, Power S (2020). Insights From CMIP6 for Australia's Future Climate. Earth's Future 8(5), e2019EF001469.

Guo Z, Still CJ, Lee CKF, Ryu Y, Blonder B, Wang J, Bonebrake TC, Hughes A, Li Y, Yeung HCH, Zhang K, Law YK, Lin Z, Wu J (2022a). Does plant ecosystem thermoregulation occur? An extratropical assessment at different spatial and temporal scales. New Phytologist nph.18632.

Guo Z, Yan Z, Majcher BM, Lee CK, Zhao Y, Song G, Wang B, Wang X, Deng Y, Michaletz ST, Ryu Y, Ashton LA, Lam HM, Wong MS, Liu L, Wu J (2022b). Dynamic biotic controls of leaf thermoregulation across the diel timescale. Agricultural and Forest Meteorology 315, 108827.

Hansen J, Ruedy R, Sato M, Lo K (2010). Global Surface Temperature Change. Reviews of Geophysics 48(4).

Hersbach H, Bell B, Berrisford P, Biavati G, Horányi A, Muñoz Sabater J, Nicolas J, Peubey C, Radu R, Rozum I, Schepers D, Simmons A, Soci C, Dee D, Thépaut JN (2018). ERA5 hourly data on single levels from 1940 to present. Copernicus Climate Change Service (C3S) Climate Data Store (CDS).

Iqbal M (1983). An Introduction to Solar Radiation. Academic Press, Toronto ; New York.

Janka E, Körner O, Rosenqvist E, Ottosen CO (2016). A coupled model of leaf photosynthesis, stomatal conductance, and leaf energy balance for chrysanthemum (Dendranthema grandiflora). Computers and Electronics in Agriculture 123, 264–274.

Jarvis PG (1976). The Interpretation of the Variations in Leaf Water Potential and Stomatal Conductance Found in Canopies in the Field. Philosophical Transactions of the Royal Society of London Series B, Biological Sciences 273(927), 593–610.

Jones HG (2013). Plants and Microclimate: A Quantitative Approach to Environmental Plant Physiology. Cambridge University Press, 3 edition.

Kullberg AT, Feeley KJ (2022). Limited acclimation of leaf traits and leaf temperatures in a subtropical urban heat island. Tree Physiology tpac066.

Kullberg AT, Slot M, Feeley KJ (2023). Thermal optimum of photosynthesis is controlled by stomatal conductance and does not acclimate across an urban thermal gradient in six subtropical tree species. Plant, Cell & Environment 46(3), 831–849.

Kunert N, Hajek P, Hietz P, Morris H, Rosner S, Tholen D (2022). Summer temperatures reach the thermal tolerance threshold of photosynthetic decline in temperate conifers. Plant Biology 24(7), 1254–1261.

Lee AP, Upchurch G, Murchie EH, Lomax BH (2015). Leaf energy balance modelling as a tool to infer habitat preference in the early angiosperms. Proceedings of the Royal Society B: Biological Sciences 282(1803), 20143052.

Leigh A, Sevanto S, Close J, Nicotra A (2017). The influence of leaf size and shape on leaf thermal dynamics: Does theory hold up under natural conditions? Plant, Cell & Environment 40(2), 237–248.

Lin YS, Medlyn BE, Duursma RA, Prentice IC, Wang H, Baig S, Eamus D, de Dios VR, Mitchell P, Ellsworth DS, de Beeck MO, Wallin G, Uddling J, Tarvainen L, Linderson ML, Cernusak LA, Nippert JB, Ocheltree TW, Tissue DT, Martin-StPaul NK, Rogers A, Warren JM, De Angelis P, Hikosaka K, Han Q, Onoda Y, Gimeno TE, Barton CVM, Bennie J, Bonal D, Bosc A, Löw M, Macinins-Ng C, Rey A, Rowland L, Setterfield SA, Tausz-Posch S, Zaragoza-Castells J, Broadmeadow MSJ, Drake JE, Freeman M, Ghannoum O, Hutley LB, Kelly JW, Kikuzawa

K, Kolari P, Koyama K, Limousin JM, Meir P, Lola da Costa AC, Mikkelsen TN, Salinas N, Sun W, Wingate L (2015). Optimal stomatal behaviour around the world. Nature Climate Change 5(5), 459–464.

Liu BYH, Jordan RC (1960). The interrelationship and characteristic distribution of direct, diffuse and total solar radiation. Solar Energy 4(3), 1–19.

Lloyd J, Farquhar GD (2008). Effects of rising temperatures and [CO2] on the physiology of tropical forest trees. Philosophical Transactions of the Royal Society B: Biological Sciences 363(1498), 1811–1817.

Mau AC, Reed SC, Wood TE, Cavaleri MA (2018). Temperate and Tropical Forest Canopies are Already Functioning beyond Their Thermal Thresholds for Photosynthesis. Forests 9(1), 47.

McColl KA (2020). Practical and Theoretical Benefits of an Alternative to the Penman-Monteith Evapotranspiration Equation. Water Resources Research 56(6), e2020WR027106.

Medlyn BE, Duursma RA, Eamus D, Ellsworth DS, Prentice IC, Barton CVM, Crous KY, De Angelis P, Freeman M, Wingate L (2011). Reconciling the optimal and empirical approaches to modelling stomatal conductance: RECONCILING OPTIMAL AND EMPIRICAL STOMATAL MODELS. Global Change Biology 17(6), 2134–2144.

Meyers TP, Paw U KT (1987). Modelling the plant canopy micrometeorology with higher-order closure principles. Agricultural and Forest Meteorology 41(1), 143–163.

Michaletz ST, Weiser MD, McDowell NG, Zhou J, Kaspari M, Helliker BR, Enquist BJ (2016). The energetic and carbon economic origins of leaf thermoregulation. Nature Plants 2(9), 16129.

Michaletz ST, Weiser MD, Zhou J, Kaspari M, Helliker BR, Enquist BJ (2015). Plant Thermoregulation: Energetics, Trait–Environment Interactions, and Carbon Economics. Trends in Ecology & Evolution 30(12), 714–724.

Miller BD, Carter KR, Reed SC, Wood TE, Cavaleri MA (2021). Only sun-lit leaves of the uppermost canopy exceed both air temperature and photosynthetic thermal optima in a wet tropical forest. Agricultural and Forest Meteorology 301–302, 108347.

Monteith J, Unsworth M (2013). Principles of Environmental Physics: Plants, Animals, and the Atmosphere. Academic Press.

Monteith JL (1965). Evaporation and Environment. In Fogg, G. E. (Ed.), The State and Movement of Water in Living Organisms, 205–234. Cambridge, UK: Cambridge University Press.

Moore CE, Meacham-Hensold K, Lemonnier P, Slattery RA, Benjamin C, Bernacchi CJ, Lawson T, Cavanagh AP (2021). The effect of increasing temperature on crop photosynthesis: From enzymes to ecosystems. Journal of Experimental Botany 72(8), 2822–2844.

Murray FW (1967). On the Computation of Saturation Vapor Pressure. Journal of Applied Meteorology and Climatology 6(1), 203–204.

New M, Lister D, Hulme M, Makin I (2002). A high-resolution data set of surface climate over global land areas. Climate Research 21, 1–25.

O'Neill BC, Tebaldi C, van Vuuren DP, Eyring V, Friedlingstein P, Hurtt G, Knutti R, Kriegler E, Lamarque JF, Lowe J, Meehl GA, Moss R, Riahi K, Sanderson BM (2016). The Scenario Model Intercomparison Project (ScenarioMIP) for CMIP6. Geoscientific Model Development 9(9), 3461–3482.

O'sullivan OS, Heskel MA, Reich PB, Tjoelker MG, Weerasinghe LK, Penillard A, Zhu L, Egerton JJG, Bloomfield KJ, Creek D, Bahar NHA, Griffin KL, Hurry V, Meir P, Turnbull MH, Atkin OK (2017). Thermal limits of leaf metabolism across biomes. Global Change Biology 23(1), 209–223.

Pan Y, Birdsey RA, Fang J, Houghton R, Kauppi PE, Kurz WA, Phillips OL, Shvidenko A, Lewis SL, Canadell JG, Ciais P, Jackson RB, Pacala SW, McGuire AD, Piao S, Rautiainen A, Sitch S, Hayes D (2011). A Large and Persistent Carbon Sink in the World's Forests. Science 333(6045), 988–993.

Penman HL (1948). Natural evaporation from open water, bare soil and grass. Proceedings of the Royal Society of London Series A Mathematical and Physical Sciences 193(1032), 120–145.

Perez TM, Feeley KJ (2020). Photosynthetic heat tolerances and extreme leaf temperatures. Functional Ecology 34(11), 2236–2245.

Premugh V (2020). The Upper Temperature Limits of Leaf Function in Tropical Trees from a Wet Tropical Forest. Master's thesis, Indian Institute of Science Education and Research, Pune.

Rahmstorf S, Foster G, Cahill N (2017). Global temperature evolution: Recent trends and some pitfalls. Environmental Research Letters 12(5), 054001.

Reda I, Andreas A (2008). Solar Position Algorithm for Solar Radiation Applications (Revised). Technical Report NREL/TP-560-34302, 15003974.

Rey-Sánchez AC, Slot M, Posada JM, Kitajima K (2016). Spatial and seasonal variation in leaf temperature within the canopy of a tropical forest. Climate Research 71(1), 75–89.

Richardson AD, Aubrecht DM, Basler D, Hufkens K, Muir CD, Hanssen L (2021). Developmental changes in the reflectance spectra of temperate deciduous tree leaves and implications for thermal emissivity and leaf temperature. New Phytologist 229(2), 791–804.

Sastry A, Barua D (2017). Leaf thermotolerance in tropical trees from a seasonally dry climate varies along the slow-fast resource acquisition spectrum. Scientific Reports 7(1), 11246.

Schymanski SJ, Or D (2017). Leaf-scale experiments reveal an important omission in the Penman–Monteith equation. Hydrology and Earth System Sciences 21(2), 685–706.

Shukla KN, Rangnekar S, Sudhakar K (2015). Comparative study of isotropic and anisotropic sky models to estimate solar radiation incident on tilted surface: A case study for Bhopal, India. Energy Reports 1, 96–103.

Slot M, Cala D, Aranda J, Virgo A, Michaletz ST, Winter K (2021). Leaf heat tolerance of 147 tropical forest species varies with elevation and leaf functional traits, but not with phylogeny. Plant, Cell & Environment 44(7), 2414–2427.

Smith MN, Taylor TC, van Haren J, Rosolem R, Restrepo-Coupe N, Adams J, Wu J, de Oliveira RC, da Silva R, de Araujo AC, de Camargo PB, Huxman TE, Saleska SR (2020). Empirical evidence for resilience of tropical forest photosynthesis in a warmer world. Nature Plants 6(10), 1225–1230.

Song Q, Sun C, Deng Y, Bai H, Zhang Y, Yu H, Zhang J, Sha L, Zhou W, Liu Y (2020). Tree Surface Temperature in a Primary Tropical Rain Forest. Atmosphere 11(8), 798.

Stewart JB (1988). Modelling surface conductance of pine forest. Agricultural and Forest Meteorology 43(1), 19–35.

Still CJ, Page G, Rastogi B, Griffith DM, Aubrecht DM, Kim Y, Burns SP, Hanson CV, Kwon H, Hawkins L, Meinzer FC, Sevanto S, Roberts D, Goulden M, Pau S, Detto M, Helliker B, Richardson AD (2022). No evidence of canopy-scale leaf thermoregulation to cool leaves below air temperature across a range of forest ecosystems. Proceedings of the National Academy of Sciences 119(38), e2205682119.

Tattersall G (2021). Gtatters/Thermimage: Thermimage v4.1.3. Zenodo.

Team RC (2021). R: A Language and Environment for Statistical Computing. R Foundation for Statistical Computing.

Tennekes H (1973). The Logarithmic Wind Profile.

Tiwari R, Gloor E, da Cruz WJA, Schwantes Marimon B, Marimon-Junior BH, Reis SM, de Souza IA, Krause HG, Slot M, Winter K, Ashley D, Béu RG, Borges CS, Da Cunha M, Fauset S, Ferreira LDS, Gonçalves MDA, Lopes TT, Marques EQ, Mendonça NG, Mendonça NG, Noleto PT, de Oliveira CHL, Oliveira MA, Pireda S, dos Santos Prestes NCC, Santos DM, Santos EB, da Silva ELS, de Souza IA, de Souza LJ, Vitória AP, Foyer CH, Galbraith D (2021). Photosynthetic quantum efficiency in south-eastern Amazonian trees may be already affected by climate change. Plant, Cell & Environment 44(7), 2428–2439.

Trenberth K (2011). Changes in precipitation with climate change. Climate Research 47(1), 123–138.

Tserej O, Feeley KJ (2021). Variation in leaf temperatures of tropical and subtropical trees are related to leaf thermoregulatory traits and not geographic distributions. Biotropica 53(3), 868–878.

Vialet-Chabrand S, Lawson T (2019). Dynamic leaf energy balance: Deriving stomatal conductance from thermal imaging in a dynamic environment. Journal of Experimental Botany 70(10), 2839–2855.

Williams SE, Bolitho EE, Fox S (2003). Climate change in Australian tropical rainforests: An impending environmental catastrophe. Proceedings

of the Royal Society of London Series B: Biological Sciences 270(1527), 1887–1892.

Yang X, Li R, Jablonski A, Stovall A, Kim J, Yi K, Ma Y, Beverly D, Phillips R, Novick K, Xu X, Lerdau M (2023). Leaf angle as a leaf and canopy trait: Rejuvenating its role in ecology with new technology. Ecology Letters 26(6), 1005–1020.

Appendix A

Supplementary figures

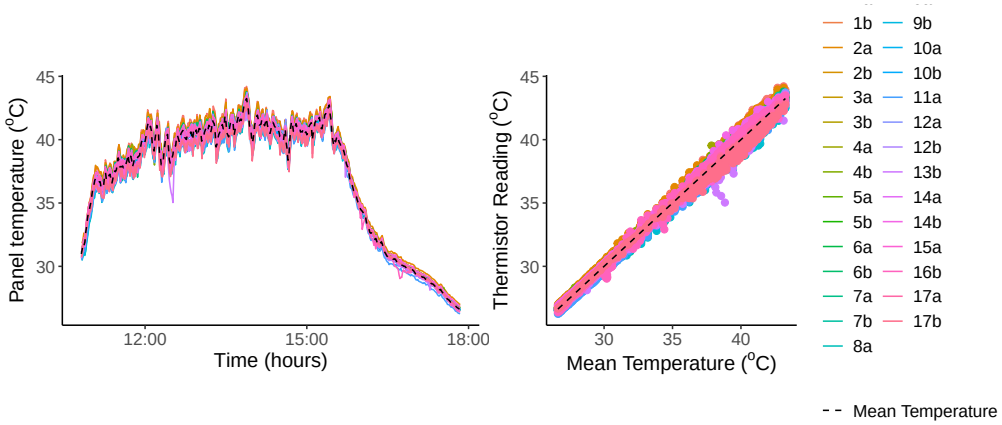

Figure A.1: **Temporal trace of the panel temperature measurements used in calibration.** The colored lines/points are different thermistor heads, and the dotted line in the left figure is the mean temperature.

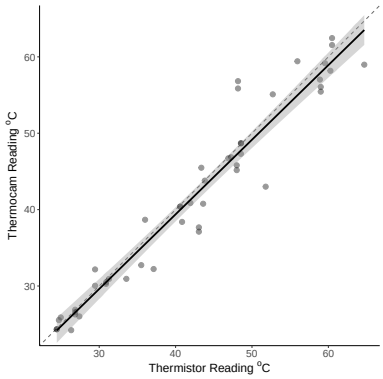

Figure A.2: **Calibration of the handheld thermal camera.** Images were taken of high-emissivity panel attached with thermistors. The line represents an ordinary least squares linear regression with standard error as the grey shade. Temperatures were then extracted by drawing a mask layer around the leaf boundary using R (Team, 2021) and Thermimage package (Tattersall, 2021).

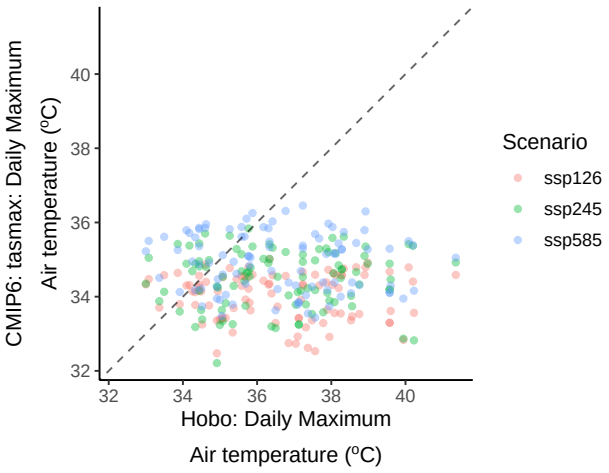

Figure A.3: **Comparison of daily maximum air temperature measured at the site and CMIP6 - tasmax.** The points are several days of the Summer of 2023 and the colors are the different scenarios from CMIP6 - SSP126, SSP245 and SSP585.

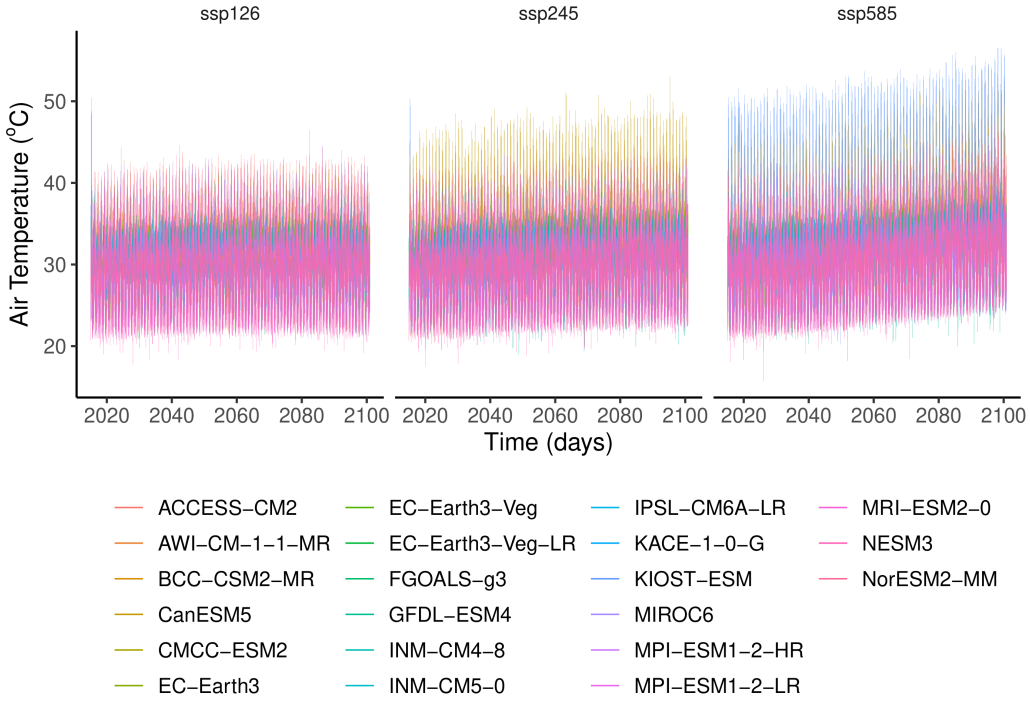

Figure A.4: **CMIP6 model outputs from multiple experiments under different Scenarios - SSP126, SSP245, and SSP585.** Colors are the different sources that produced the outputs. The data shown in Fig. 4.2 were calculated by taking the daily means of these outputs.